AGU PUBLICATIONS

Water Resources Research

RESEARCH ARTICLE
10.1002/2014WR015331

Companion to *Chiogna et al.* [2015], doi:10.1002/2014WR015330.

**Key Points:**
- Natural sediments exhibit nonstationary anisotropic structures
- Nonstationary anisotropy causes secondary groundwater motion
- Secondary motion enhances transverse mixing and dilution

**Supporting Information:**
- Readme
- movie_nonstationaryms01.gif
- movie_stationaryms02.gif

**Correspondence to:**
O. A. Cirpka,
olaf.cirpka@uni-tuebingen.de

**Citation:**
Cirpka, O. A., G. Chiogna, M. Rolle, and A. Bellin (2015), Transverse mixing in three-dimensional nonstationary anisotropic heterogeneous porous media, *Water Resour. Res.*, *51*, 241–260, doi:10.1002/2014WR015331.

Received 20 JAN 2014
Accepted 1 DEC 2014
Accepted article online 5 DEC 2014
Published online 12 JAN 2015

# Transverse mixing in three-dimensional nonstationary anisotropic heterogeneous porous media

**Olaf A. Cirpka[1], Gabriele Chiogna[1], Massimo Rolle[1,2,3], and Alberto Bellin[4]**

[1]Center for Applied Geoscience, University of Tübingen, Tübingen, Germany, [2]Department of Civil and Environmental Engineering, Stanford University, Stanford, California, USA, [3]Now at Department of Environmental Engineering, Technical University of Denmark, Lyngby, Denmark, [4]Department of Civil, Environmental and Mechanical Engineering, University of Trento, Trento, Italy

**Abstract** Groundwater plumes originating from continuously emitting sources are typically controlled by transverse mixing between the plume and reactants in the ambient solution. In two-dimensional domains, heterogeneity causes only weak enhancement of transverse mixing in steady-state flows. In three-dimensional domains, more complex flow patterns are possible because streamlines can twist. In particular, spatially varying orientation of anisotropy can cause steady-state groundwater whirls. We analyze steady-state solute transport in three-dimensional locally isotropic heterogeneous porous media with blockwise anisotropic correlation structure, in which the principal directions of anisotropy differ from block to block. For this purpose, we propose a transport scheme that relies on advective transport along streamlines and transverse-dispersive mass exchange between them based on Voronoi tessellation. We compare flow and transport results obtained for a nonstationary anisotropic log-hydraulic conductivity field to an equivalent stationary field with identical mean, variance, and two-point correlation function disregarding the nonstationarity. The nonstationary anisotropic field is affected by mean secondary motion and causes neighboring streamlines to strongly diverge, which can be quantified by the two-particle semivariogram of lateral advective displacements. An equivalent kinematic descriptor of the flow field is the advective folding of plumes, which is more relevant as precursor of mixing than stretching. The separation of neighboring streamlines enhances transverse mixing when considering local dispersion. We quantify mixing by the flux-related dilution index, which is substantially larger for the nonstationary anisotropic conductivity field than for the stationary one. We conclude that nonstationary anisotropy in the correlation structure has a significant impact on transverse plume deformation and mixing. In natural sediments, contaminant plumes most likely mix more effectively in the transverse directions than predicted by models that neglect the nonstationarity of anisotropy.

## 1. Introduction

Mixing processes in geologic formations play a pivotal role in determining the fate of contaminants and the evolution of groundwater quality. Insufficient mixing of reactants often limits the overall rates of (bio)geochemical reactions. Therefore, understanding and quantifying the complex interaction between mixing and transformation processes is of utmost importance to describe contaminant transport and natural attenuation in subsurface environments [e.g., *Kitanidis and McCarty*, 2012; *Dentz et al.*, 2011]. In particular, for plumes evolving from continuous sources, transverse dispersion, which acts in the directions perpendicular to flow, represents the main mixing mechanism and a fundamental controlling factor for the evolution of groundwater plumes [e.g., *Cirpka et al.*, 1999a]. The key physical process leading to transverse solute mixing is the mass exchange between adjacent streamtubes, which results in dilution of a solute plume and in the increase of its entropy [*Kitanidis*, 1994; *Chiogna et al.*, 2011b, 2012], in the reduction of the peak concentration and the concentration variance [e.g., *Pannone and Kitanidis*, 1999; *Fiori*, 2001; *Tonina and Bellin*, 2008; *Vanderborght*, 2001], and affects the evolution of statistical concentration distributions [*Schwede et al.*, 2008; *Bellin and Tonina*, 2007; *Caroni and Fiorotto*, 2005]. For reactive transport in groundwater, transverse mixing allows the reaction between dissolved contaminants and reactants transported in the ambient water and, in presence of sufficiently fast degradation kinetics, controls the length of steady-state plumes [e.g., *Liedl et al.*, 2005, 2011; *Cirpka et al.*, 2012, 2006; *Cirpka and Valocchi*, 2007, 2009]. As shown by modeling studies

[e.g., *Cirpka et al*., 1999a; *Prommer et al*., 2009] and experimental investigations both at laboratory and field scales [e.g., *Davis et al*., 1999; *Thornton et al*., 2001; *Anneser et al*., 2008; *Bauer et al*., 2009a], narrow zones with high concentration gradients develop at the side of reactive groundwater plumes. In such fringe zones, mass transfer is enhanced, and favorable conditions for biogeochemical reactions occur.

Conservative and reactive mixing in groundwater are greatly influenced by the heterogeneous nature of geologic formations and, in particular, by the spatial variability of physical properties in aquifer systems. The influence of spatially variable hydraulic conductivity on flow and solute transport has been extensively studied by stochastic theory [e.g., *Dagan*, 1989; *Gelhar*, 1993; *Rubin*, 2003]. Closed-form expressions for metrics of flow and transport in heterogeneous media have mainly been derived for statistically stationary formations with locally isotropic hydraulic conductivity. In these approaches, the statistical descriptors of the log-hydraulic conductivity field, in particular the mean and covariance function, are considered invariant in space.

From a practical standpoint of view, it is already difficult to estimate stationary statistical parameters from field surveys, so that any attempt of addressing nonstationarity beyond simple linear trends of the mean [e.g., *Rubin*, 2003, sections 4.2.2 and 5.7] appears unrealistic for a given field site, not to mention the derivation of closed-form expressions. Conversely, texturally rich sedimentary deposits show internal structures that hardly resemble multi-Gaussian, second-order stationary random fields analyzed by classical stochastic subsurface hydrology [e.g., *Heinz et al*., 2003; *Bayer et al*., 2011]. As reviewed in section 2.5 of *Rubin* [2003], several approaches have been proposed to characterize the architecture of complex sedimentary units, e.g., as hierarchy of units that are statistically described by transition probabilities [e.g., *Carle and Fogg*, 1997] and exhibit internal variability described by second-order geostatistics. *Ritzi et al*. [2004] approached the problem by using a hierarchy of geometric bodies. While some studies have focused on deriving equivalent stationary log-conductivity, flow, and transport properties from such characterizations [e.g., *Rubin*, 1995; *Dai et al*., 2004], the focus of the present study and the companion paper of *Chiogna et al.* [2015] lies on demonstrating that important flow and transport features are lost by the derivation of equivalent stationary properties. In particular, we are interested in the effects of spatially varying orientation of statistical anisotropy on solute mixing which, as stated above, controls the length of (quasi) steady-state plumes.

The focus of stochastic analysis of groundwater transport has been mainly the study of the concentration's spatial moments to determine dispersion in heterogeneous media. Stochastic approaches define the ensemble dispersion tensor as half the rate of increase of the second central moments of the ensemble concentrations [e.g., *Gelhar and Axness*, 1983; *Dagan*, 1984; *Neuman et al*., 1987], and the effective dispersion tensor by the ensemble average of half the rate of change in the second central moments of plumes in individual realization, that is, the two dispersion tensors differ in the order of computing spatial moments and averaging over all realizations [e.g., *Kitanidis*, 1988; *Dagan*, 1991; *Rajaram and Gelhar*, 1995; *Dentz et al*., 2000a; *Dentz and Carrera*, 2003]. Although useful for the description of plume evolution, such parameters do not allow a proper quantification of actual mixing processes in heterogeneous formations. Recently, *Cirpka et al*. [2011] proposed an approach for two-dimensional heterogeneous porous media based on flux-related second central moments, which focuses on transverse mixing and adopts a stochastic flux-related framework. This approach allows defining a mixing-relevant transverse dispersion coefficient exclusively accounting for the actual mass exchange between streamtubes, without being affected by advective processes which lead to plume meandering, squeezing, and stretching.

Investigations on transverse mixing have been carried out using a variety of approaches such as analytical and numerical studies [e.g., *Cirpka and Kitanidis*, 2000; *de Barros and Nowak*, 2010; *Chiogna et al*., 2011a; *Rolle et al*., 2013], pore-scale simulations [*Acharya et al*., 2007; *Rolle et al*., 2012; *Hochstetler et al*., 2013], and experimental investigations including microfluidic experiments [*Willingham et al*., 2008; *Zhang et al*., 2010] and laboratory flow-through setups [e.g., *Rahman et al*., 2005; *Bauer et al*., 2009b; *Chiogna et al*., 2010]. A common feature of these studies is that they were performed in two-dimensional or quasi two-dimensional systems. Under such conditions, the main process by which heterogeneity in hydraulic conductivity influences transverse mixing is the convergence and divergence of streamlines. As illustrated by *Werth et al*. [2006], flow focusing in high-conductivity inclusions results in consistent mixing enhancement because the transverse mixing lengths of dispersion are reduced in these inclusions.

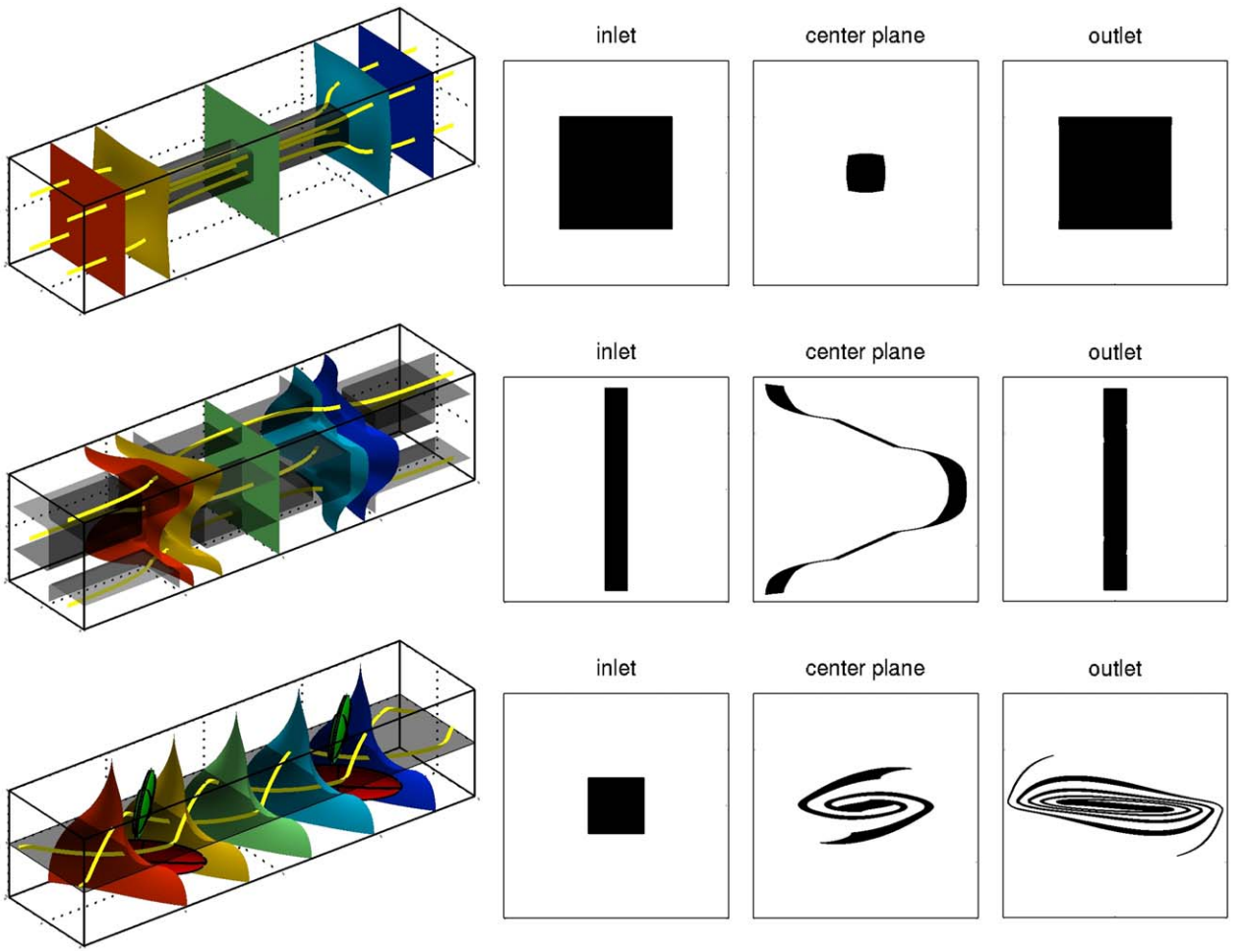


**Figure 1.** Illustration of the effects of heterogeneity and anisotropy in 3-D flow fields on solute transport: potential surfaces, streamlines, and plume cross sections for purely advective transport. (a) Flow-focusing effect of a single high-permeability inclusion (gray body); (b) depth-dependent meandering due to 3-D architecture of high-permeability zones (gray bodies); and (c) streamline twisting in bounded layer-wise homogeneous anisotropic fields (gray surface: interface between two layers with different anisotropy orientations).

In three-dimensional heterogeneous media, the study of flow and transport processes becomes more challenging. In fact, in such media, groundwater flow may exhibit a complex flow topology. In particular, *Bakker and Hemker* [2004], *Hemker and Bakker* [2006], and *Stauffer* [2007] showed how anisotropy of hydraulic conductivity can lead to groundwater whirls which may affect solute mixing in ways that are impossible in two-dimensional domains. Recent studies on solute transport in complex three-dimensional setups include the work on macrodispersion by *Jankovic et al*. [2009] and *de Dreuzy and Beaudoin* [2013], and the studies of solute breakthrough of *Fiori et al*. [2011] and *Zarlenga et al*. [2013]. *Stauffer and Rauber* [1998] analyzed macrodispersion in virtual hierarchical sedimentary structures generated by hydrofacies modeling followed by filling the sedimentary structures with blockwise stationary anisotropic log conductivity field.

To the best of our knowledge, no investigation has yet addressed transverse mixing in three-dimensional locally isotropic heterogeneous porous media with nonstationary anisotropic correlation structure. In such complex 3-D systems, additional mechanisms compared to those occurring in 2-D setups can cause significant mixing enhancement. Figure 1 illustrates three main mechanisms enhancing mixing in 3-D porous media. Figure 1a shows flow focusing in a high-permeability inclusion which results in increased mass transfer between adjacent streamlines. This process also occurs in 2-D flows [e.g., *Werth et al*., 2006; *Cirpka et al*., 2011]. Mixing enhancement can also occur through depth-dependent meandering, which results in deformation of the plume surface thus causing an increased interfacial area and enhanced transverse mass fluxes (Figure 1b). Finally, in heterogeneous anisotropic media, groundwater flow can show secondary motion,

consisting in persistent flow components determined by the large-scale hydraulic gradient, which overlay the primary velocity field. Secondary motion may involve twisting, folding, and intertwining of streamlines (Figure 1c), which may have a dramatic impact on mixing. The present study focuses on the last aspect. In this work the term "anisotropic," does not refer to the local hydraulic conductivity tensor as done by *Bakker and Hemker* [2004], *Hemker and Bakker* [2006], and *Stauffer* [2007], but to the covariance function of the random (scalar) log-hydraulic conductivity field.

The evaluation of transverse mixing in heterogeneous porous media poses a specific challenge for numerical simulations. While particle-tracking methods are particularly well suited to simulate advective transport without introduction of numerical dispersion, they typically handle pore-scale dispersion by a random walk, requiring many particles to be released in order to obtain good statistics and facilitate the computation of reliable concentrations [*Tonina and Bellin*, 2008; *Boso et al*., 2013]. In strictly Eulerian methods, which are well suited to simulate dispersion, the approximation of advection may lead to severe artificial transverse mixing due to grid-orientation effects. In two-dimensional steady-state flows, *Cirpka et al*. [1999b, 1999c] constructed streamline-oriented grids and solved advective-dispersive transport by the Finite Volume method. While this approach suppressed artificial transverse dispersion, it can only be transferred to three-dimensional domains in cases of simple flow topology exhibiting no twisting streamlines. Recently, *Herrera et al*. [2010] suggested to solve advective transport and excess longitudinal dispersion along streamlines, and approximate the remaining isotropic dispersion by smoothed-particle hydrodynamics. *Boso et al*. [2013] showed that smoothed-particle hydrodynamics is free of numerical diffusion, but the accuracy attained in the dispersive Eulerian step of the procedure deteriorates when the spatial distribution of particles becomes progressively less uniform. This forces to increase the number of particles with increasing heterogeneity of the formation. In the present study, we solve advection by streamline-transport (particle tracking), but we simulate transverse dispersion by the Finite Volume method using Voronoi tessellation, rather than relying on smoothed-particle hydrodynamics.

The quantitative assessment of transverse mixing and its enhancement in three-dimensional heterogeneous anisotropic porous media are the main goal of the present work. To achieve this, we consider scalar heterogeneous hydraulic conductivity fields with blockwise stationary anisotropic correlation function. Flow in such three-dimensional domains exhibits a complex topology characterized by large-scale secondary motion overlain by small-scale variability. Such small-scale variability causes flow focusing and promotes mass exchange between streamlines that, in the presence of secondary motion, proceed in substantially different directions, thus enhancing transverse mixing of the solute in three-dimensional domains. A detailed discussion of the flow topology in such heterogeneous anisotropic fields and of the complex patterns of computed streamlines are presented in the companion paper of *Chiogna et al.* [2015]. The specific research objectives of this study are to (i) demonstrate and quantify the effect of secondary flow caused by nonstationary anisotropy of the log-hydraulic conductivity field on steady-state transverse mixing in 3-D heterogeneous anisotropic porous media, using the flux-related dilution index as metric of mixing [*Rolle et al*., 2009]; (ii) relate the observed mixing enhancement to the moments of advective particle displacement; (iii) test whether metrics of advective stretching and folding, discussed in *Chiogna et al.* [2015], are good descriptors for the facilitation of mixing; (iv) identify and separate the effects of flow-focusing and secondary motion by performing comparative studies with equivalent stationary fields; (v) develop and apply a numerical method that allows studying transverse mixing without artifacts caused by the discretization of advective transport. Finding upscaling rules for mixing in flow fields affected by nonstationary anisotropy should be the ultimate goal in this line of research but is still beyond the scope of the present contribution.

## 2. Mathematical Formulation

### 2.1. Flow in Periodic Porous Media

In the following analysis, we consider an infinite, three-dimensional, periodic, porous medium, in which hydraulic conductivity $K$ [$L\,T^{-1}$] repeats its values in the spatial $x$-, $y$-, and $z$-directions [$L$] at distances of $L\times W\times H$ [$L$]. The logarithm of hydraulic conductivity, ln $K$, is assumed to be a periodic random space function with uniform mean and blockwise second-order stationary, anisotropic covariance function.

The specific discharge or Darcy velocity $\mathbf{q}$ [$L\,T^{-1}$] at steady-state is governed by the continuity equation:

$$\nabla \cdot \mathbf{q} = 0 \tag{1}$$

considered here in the absence of sources and sinks and with $\mathbf{q}$ obeying Darcy's law:

$$\mathbf{q} = -\mathbf{K} \cdot \nabla h \tag{2}$$

where $h(\boldsymbol{x})$ $[L]$ denotes hydraulic head and $\boldsymbol{x} = (x,y,z)$ $[L]$ is the vector of spatial coordinates. $\mathbf{K}$ is assumed to be locally isotropic, so that $\mathbf{K}$ becomes a scalar field $K(\boldsymbol{x})$.

To obtain the flow field in the infinite domain, stressed by a uniform-in-the-mean negative hydraulic gradient $\boldsymbol{J} = [J_x, J_y, J_z]$[-], it is sufficient to consider a single unit cell with dimensions $L \times W \times H$ and apply periodic head conditions with a mean hydraulic gradient to the external surfaces of the unit cell domain [e.g., *Kitanidis*, 1992]:

$$h(L,y,z) = h(0,y,z) - L \cdot J_x \tag{3}$$

$$h(x,W/2,z) = h(x,-W/2,z) - W \cdot J_y \tag{4}$$

$$h(x,y,H/2) = h(x,y,-H/2) - H \cdot J_z \tag{5}$$

in which $\mathbf{J}$ is chosen such that the volume-averaged Darcy velocity $\overline{\mathbf{q}}$ is oriented along the $x$-direction and the absolute value of $\mathbf{J}$ meets a predefined value. Due to the periodic head boundary conditions and the periodic conductivity field, the head and velocity fields in the infinite domain are periodic, too:

$$h(x+iL_x, y+jL_y, z+kL_z) = h(x,y,z)\ \forall i,j,k \in \mathbb{Z}, x,y,z \in \mathbb{R} \tag{6}$$

$$\mathbf{q}(x+iL_x, y+jL_y, z+kL_z) = \mathbf{q}(x,y,z)\ \forall i,j,k \in \mathbb{Z}, x,y,z \in \mathbb{R} \tag{7}$$

For the following numerical analysis, the $x$-component of the velocity must be positive everywhere: $v_x > 0,\ \forall \mathbf{x}$. Although it cannot be excluded a priori, the emergence of a local negative $v_x$-value is a rare event, in particular in weakly heterogeneous formations, and a posteriori we verified that the resulting velocity field meets this condition.

### 2.2. Solute Transport

Solute transport in groundwater is commonly described by the advection-dispersion equation (ADE):

$$\frac{\partial c}{\partial t} + \mathbf{v} \cdot \nabla c - \nabla \cdot (\mathbf{D} \nabla c) = 0, \tag{8}$$

in which $c$ $[M\ L^{-3}]$ is the solute concentration of a compound here assumed conservative, $t$ $[T]$ is time, $\boldsymbol{v} = \boldsymbol{q}/\theta$ $[L\ T^{-1}]$ is the seepage-velocity vector, related to Darcy velocity $\mathbf{q}$ through the porosity $\theta$, and $\mathbf{D}$ $[L^2\ T^{-1}]$ is the local dispersion tensor. The term "local" implies that velocity fluctuations are averaged only at the pore scale at which Darcy's law does not hold anyway, whereas the variation of the Darcy velocity $\mathbf{q}$ is resolved as well as possible.

The local dispersion tensor $\mathbf{D}$ assumes the following general expression [*Bear*, 1972, chapter 10.4]:

$$\mathbf{D} = \frac{\mathbf{v} \otimes \mathbf{v}}{\mathbf{v} \cdot \mathbf{v}} (D_\ell - D_t) + \mathbf{I} D_t, \tag{9}$$

in which $\mathbf{v} \otimes \mathbf{v}$ and $\boldsymbol{v} \cdot \boldsymbol{v}$ denote the tensor and scalar products of $\mathbf{v}$ with itself, respectively, and $\mathbf{I}$ is the identity matrix. $D_\ell$ $[L^2\ T^{-1}]$ and $D_t$ $[L^2\ T^{-1}]$ are the longitudinal and transverse dispersion coefficients, respectively.

For transport, we consider a semi-infinite subdomain, starting at the inlet face at the plane $x = 0$. Here we assume as boundary condition for equation (8) a fixed concentration distribution $c_{fix}(y,z)$ $[M\ L^3]$:

$$c = c_{fix}(y,z) \ \text{ at } \ x = 0, \tag{10}$$

and periodic boundary conditions at the other external surfaces, which ensure that the boundary conditions only minimally influence the concentration distribution.

At a sufficiently long time with constant inlet concentration $c_{fix}$, the concentration field approaches steady-state. Then, at a sufficiently large distance from the inlet, equation (8) can be simplified to

$$v_x \frac{\partial c}{\partial x} + v_y \frac{\partial c}{\partial y} + v_z \frac{\partial c}{\partial z} - \frac{\partial}{\partial y}\left(D_t \frac{\partial c}{\partial y}\right) - \frac{\partial}{\partial z}\left(D_t \frac{\partial c}{\partial z}\right) = 0, \tag{11}$$

in which longitudinal dispersion has been neglected because at steady-state dispersive mass flux varies mainly in the transverse directions [e.g., *Zarlenga and Fiori*, 2013]. For uniform flow, *Wexler* [1992] gives $Pe = vx/D_\ell > 30$ as criterion to neglect longitudinal dispersion in steady-state transport. In equation (11), we have also neglected dispersive flux components in the *x*-direction because flow is predominantly oriented in this direction.

For the transverse local dispersion coefficient, we assume the standard linear model of *Scheidegger* [1961]:

$$D_t = D_p + \alpha_t |\mathbf{v}|, \tag{12}$$

in which $D_p$ [$L^2\ T^{-1}$] is the pore diffusion coefficient, and $\alpha_t$ [$L$] is the transverse dispersivity, assumed uniform. Although nonlinear and compound-specific models have been shown to be more accurate in describing local transverse dispersion [*Chiogna et al.*, 2010], the simplified linear parameterization has been selected for the ease of the following analysis.

### 2.3. Lagrangian Analysis of Steady-State Advective Transport

The advective component of the transport equation (11) can be solved by considering solute particles continuously injected trough the inlet face and moving within the velocity field along trajectories meeting the following differential equation:

$$\frac{d\mathbf{x}_p(\tau)}{d\tau} = \mathbf{v}\left(\mathbf{x}_p(\tau)\right), \tag{13}$$

$$\mathbf{x}_p(0) = (0, y_{p,0}, z_{p,0}), \tag{14}$$

in which $\boldsymbol{x}_p(\tau)$ [$L$] is the position-vector of the targeted particle $p$ at travel time $\tau$ [$T$], and $(0, y_{p,0}, z_{p,0})$ is the starting position of the particle within the vertical plane at $x = 0$, which represents the inlet surface. Given that $v_x > 0$, each particle crosses the vertical observation planes only once and a univocal correspondence can be established between the travel time $\tau$ and the longitudinal component of the particle's trajectory $\boldsymbol{x}_p$.

We now consider the transverse particle displacements $Y(x)$ [$L$] and $Z(x)$ [$L$] of each streamline at a given distance $x$ from the inlet:

$$Y(x) = y_p(\tau(x)) - y_{p,0}; \quad Z(x) = z_p(\tau(x)) - z_{p,0}, \tag{15}$$

where $\tau(x)$ is the time at which the particle $p$ crosses the vertical plane at $x$ (provided that at time $t = 0$ it started within the vertical plane at $x = 0$).

The statistics of the transverse particle displacements, in particular the variances, provide a measure of the transverse spreading of the solute and the uncertainty of plume meandering. For second-order stationary random porous media, analytical approximations of the variances of transverse displacements, $\sigma_Y^2 = E\left[(Y-\mu_Y)^2\right]$ and $\sigma_Z^2 = E\left[(Z-\mu_Z)^2\right]$, have been derived in the context of macrodispersion theory, where $E[\cdot]$ indicates statistical expectation and $\mu_Y = E[Y]$ and $\mu_Z = E[Z]$ are the expected values of $Y$ and $Z$, respectively [*Gelhar and Axness*, 1983; *Dagan*, 1984; *Neuman et al.*, 1987; *Fiori*, 1996; *Salandin and Fiorotto*, 2000, among others]. In stationary media, $\sigma_Y^2$ and $\sigma_Z^2$ increase monotonically with time, approaching a slow linear growth at large times [see *Fiori*, 1996, equation (11)].

Of higher relevance for solute mixing are the semivariograms $\gamma_Y$ [$L^2$] and $\gamma_Z$ [$L^2$] of transverse particle displacement (also known as pair dispersion), that is, half the expected value of the squared directional distance between two particles:

$$\begin{aligned} \gamma_Y(x) &= \frac{1}{2} E\left[(Y_1(x) - Y_2(x))^2\right], \\ \gamma_Z(x) &= \frac{1}{2} E\left[(Z_1(x) - Z_2(x))^2\right], \end{aligned} \tag{16}$$

in which $Y_i(x)$ and $Z_i(x)$ are the lateral displacements according to equation (15) of particle $i$ when passing the observation plane at distance $x$ from the inlet plane. $\gamma_Y(x)$ and $\gamma_Z(x)$ depend on the initial distance of the

particles considered. The major information content of $\gamma_Y(x)$ and $\gamma_Z(x)$ is how strongly two particles separate from each other by advection if local transverse dispersion makes one of the two particles jumping onto a neighboring streamline. Half the rate of change of $\gamma_Y(x)$ and $\gamma_Z(x)$ denotes the relative or effective transverse dispersion coefficient [*Andricevic and Cvetkovic*, 1998; *Attinger et al*., 2004; *Dentz et al*., 2000a, 2000b; *Fiori and Dagan*, 2000]. In a strictly advective context, i.e., in the absence of local dispersion, dilution vanishes and $\gamma_Y$ and $\gamma_Z$ are zero at all times if the two particles originate from the same position. While analytical approximations for $\gamma_Y$ and $\gamma_Z$ with zero initial distance exist for finite local dispersion tensor **D** [see *Attinger et al*., 2004; *Dentz et al*., 2000a, 2000b; *Fiori and Dagan*, 2000], we will analyze $\gamma_Y$ and $\gamma_Z$ here numerically, for small initial distances different from zero in the strictly advective regime. In addition, we consider metrics of advective stretching and folding discussed in detail in the companion paper [*Chiogna et al*. 2015].

### 2.4. Entropy-Based Analysis of Steady-State Advective-Dispersive Transport

An effective way to quantify transverse mixing within a control plane at a given longitudinal distance $x$ from the inlet plane for steady-state advective-dispersive transport is through the flux-related dilution index $E_Q(x)$ [$L^3\,T^{-1}$] [*Rolle et al*., 2009; *Chiogna et al*., 2011b]:

$$E_Q(x)=\exp\left(-\int_{-\infty}^{+\infty}\int_{-\infty}^{+\infty}p_Q(x,y,z)\ln\left(p_Q(x,y,z)\right)q_x(x,y,z)dydz\right), \tag{17}$$

in which $p_Q(x,y,z)$ [$T\,L^{-3}$] is the flux-related density of solute mass within the control plane at $x$:

$$p_Q(x,y,z)=c(x,y,z)\left(\int_{-\infty}^{+\infty}\int_{-\infty}^{+\infty}c(x,y',z')q_x(x,y',z')dy'dz'\right)^{-1} \tag{18}$$

and $q_x$ is the specific-discharge component in the $x$-direction:

$E_Q(x)$ expresses the effective volumetric flux over which the solute mass flux is distributed.

## 3. Numerical Methods

The head and velocity fields are computed by applying the cell-centered Finite Volume method to equations (1–5) with uniform grid spacing. Streamlines are then computed by particle tracking using Pollock's semianalytical approach [*Pollock*, 1988].

By following particle trajectories, $y_p(x)$ and $z_p(x)$, the advective contributions in the $y$- and $z$-direction of the steady-state transport equation (11) drop out. We pick nodes on the streamlines at a regular reciprocal distance $\Delta x$ along the longitudinal direction $x$. In each plane, polygons belonging to the nodes are constructed by Voronoi tesselation [*de Marsily*, 1986, chapter 12.2.3]. Then, integrating equation (11) over the area $A_i$ [$L^2$] of the Voronoi polygon belonging to streamline $i$, and applying the divergence theorem yields

$$\int_{A_i}v_x\frac{\partial c}{\partial x}dA-\oint_{B_i}\mathbf{n}\left(\cdot D_t\nabla_{y,z}c\right)dB=0 \tag{19}$$

in which $B_i$ [$L$] is the boundary of polygon $i$, **n** is the normal vector of the polygon within the plane pointing outwards, and $\nabla_{y,z}$ is the vector of partial derivatives in the $y$- and $z$-directions.

In the Finite Volume approach, we take the mean values of $c$ within cells as primary unknown. In the following, $c_i(x)$ denotes the concentration in the Voronoi polygon belonging to streamline $i$ within the plane at $x$. For differentiation in the $x$-direction, we apply Finite Differences. The lateral exchange is evaluated by an implicit scheme, that is, at the downstream end of a streamtube section. For the latter, we consider the concentration values in neighboring polygons $i$ and $j$, the distance $d_{i,j}$ [$L$] between the respective nodes, the length $\ell_{i,j}$ [$L$] of the common interface of the two polygons, and an average transverse dispersion coefficient $D_{i,j}$ [$L^2\,T^{-1}$]. This leads to the following balance equation:

$$\frac{c_i(x+\Delta x)-c_i(x)}{\Delta x}Q_i+\sum_{j:\text{neighbors of i}}\theta\cdot\frac{D_{i,j}\cdot\ell_{i,j}}{d_{i,j}}\bigg|_{x+\Delta x}\cdot\left(c_i(x+\Delta x)-c_j(x+\Delta x)\right)=0 \tag{20}$$

in which $Q_i$ [$L^3\,T^{-1}$] is the discharge in streamtube $i$, and $D_{i,j}$ is chosen as the harmonic average of the transverse dispersion coefficients obtained by substituting the velocities of the two streamlines $i$ and $j$ into equation (12). A schematic of the Voronoi polygons in two successive control planes is shown in Figure 2.

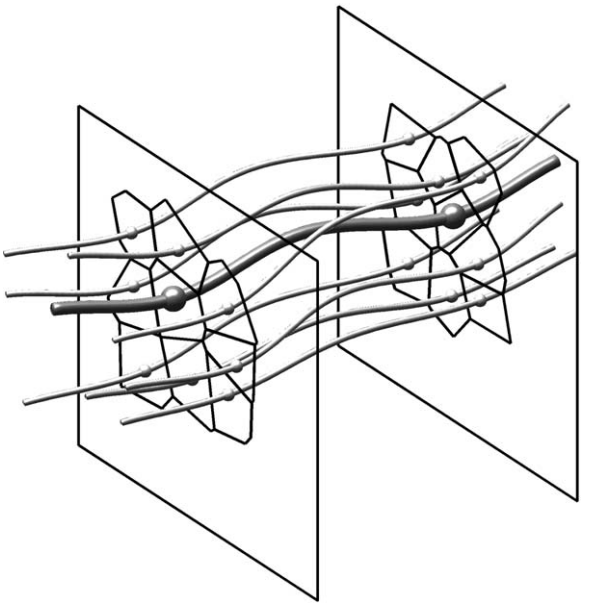

**Figure 2.** Illustration of the numerical scheme. (1) Streamlines are constructed by particle tracking. (2) Nodes are placed along the streamlines in regularly spaced observation planes orthogonal to the mean direction of flow. (3) Steady state advective dispersive transport is simulated from an observation plane to the next considering (a) the travel time along the streamline for advection and (b) transverse dispersion between the streamlines using the cell-centered Finite Volume method based on Voronoi tessellation within the observation planes.

Assembling equation (20) for all streamlines leads to a linear system of equations with symmetric positive-definite matrix. The numerical scheme is implemented in Matlab, making use of the Delaunay-triangulation class for the Voronoi tessellation, and the UMFPACK direct solver for the solution of the resulting system of equations. We have validated the method by 3-D steady-state transport examples in uniform flow and by comparison to 2-D simulations using the approach of *Cirpka et al.* [1999c].

The proposed scheme shares with smoothed-particle hydrodynamics (SPH) the idea of representing advection along streamlines, which significantly reduces numerical transverse dispersion caused by grid-orientation effects [e.g., *Cirpka et al*., 1999c], while addressing the diffusive term with an Eulerian scheme. The two approaches differ in the Eulerian scheme used to solve the diffusive part of the equation. While in smoothed-particle hydrodynamics, solute mass is exchanged between neighboring particles according to their reciprocal distance [*Herrera et al*., 2010], the method used in the present work relies on the application of the Finite Volume method to an irregular grid composed by the Voronoi polygons, thereby handling directly diffusive fluxes across streamlines. In general, the scheme presented here could be extended to a 3-D discretization of the full domain using 3-D Voronoi tessellation to construct Finite Volumes for dispersion and keeping the particle tracking to construct the streamlines.

## 4. Comparative Test Cases

The test cases are based on four interrelated velocity fields: (1) A "fully resolved" velocity field obtained by numerically solving the flow equation (1) coupled to Darcy's law, equation (2), in a single, fine discretized, periodic random log-conductivity field with nonstationary, anisotropic correlation structure, (2) a velocity field resulting from averaging an ensemble of 50 velocity fields with the same nonstationary anisotropic geostatistics as the velocity field 1, that are additionally averaged in the *x*-direction, (3) a "fully resolved" velocity field resulting from a single, fine discretized, periodic random log conductivity field with stationary correlation structure derived from case 1, and (4) a velocity field resulting from averaging an ensemble of 50 velocity fields with the same stationary geostatistics as the velocity field of case 3, that are additionally averaged in the *x*-direction.

The purpose of including the averaged velocity fields is twofold. First, we want to discriminate between effects of small-scale fluctuations of the velocity field on transverse mixing and effects caused by the large-scale secondary motion induced by nonstationary anisotropy. This is also of practical relevance as most real-world application would be based on blockwise uniform, anisotropic conductivity to represent the subsurface structure [as done by *Bakker and Hemker*, 2004; *Hemker and Bakker*, 2006; *Stauffer*, 2007] rather than generating a fine resolved log conductivity field with blockwise stationary anisotropic covariance function. The second purpose is related to flow topology. As discussed in more

detail by *Chiogna et al.* [2015], the local helicity density of the flow field in the fully resolved cases 1 and 3 is zero throughout the domain, whereas the averaged field of case 2 exhibits a nonzero local helicity density. If the pointwise evaluated helicity density was a good indicator of mixing enhancement, the dilution of case 1 had to be smaller than in case 2. We will show, however, that this is not the case. In *Chiogna et al.* [2015], we argue that the velocity field needs to be properly upscaled before computing the helicity density to make statements whether mixing enhancement by helical flow structures occurs at a given scale.

The average velocity field in the stationary case, by contrast, is added for completeness: The expected average flow field in a stationary formation driven by a uniform hydraulic gradient is uniform as well, so that we expect to see no enhancement of transverse mixing whatsoever.

The three-dimensional, heterogeneous, anisotropic log-hydraulic conductivity field of case 1 has a blockwise constant correlation structure given by the following Gaussian covariance function:

$$C_{\ln K}(\mathbf{r}) = \sigma^2_{\ln K} \exp(-r'2) \tag{21}$$

in which $r' = \sqrt{(r_1/I_1)^2 + (r_2/I_2)^2 + (r_z/I_z)^2}$, with $I_1$, $I_2$, and $I_z$ being the correlation lengths in the two principal horizontal directions $x_1$ and $x_2$, and in the vertical direction $z$, respectively. Notice that, according to the adopted model of spatial variability, the vertical direction $z$ is also a principal direction of the hydraulic conductivity tensor (i.e., $x_3 \equiv z$) and will remain fixed, while the first two principal directions will be rotated in the blocks composing the computational domain.

The geometric mean of hydraulic conductivity is $1 \times 10^{-4}$ m/s, the variance of log conductivity $\sigma^2_{\ln K}$ is 2.0, and the correlation lengths are $I_1 = 2$m, $I_2 = 0.4$ m and $I_z = 0.1$ m. The blocks are stripes of 5 m width and 1 m height, extending over the entire length of the domain in the $x$-direction. In the top left and bottom right stripes, the principal directions $x_1$ and $x_2$ of the log conductivity field are rotated by 30° to the left of the $x$- and $y$-directions, respectively. The same principal directions are rotated by 30° to the right with respect to the axes $x$ and $y$ in the top right and bottom left blocks. In each realization, two statistically independent random fields, differing by the orientation of anisotropy discussed above, are generated by the spectral approach of *Dietrich and Newsam* [1993]. The transition between the blocks is obtained by blending the two fields using a Tukey window [*Tukey*, 1967] with a transition zone of 1 m width in the $y$-direction and 0.2 m height in the $z$-direction. The dimensions of the computational domain (the unit cell that is subsequently used to generate a large velocity field) is 30 m × 10 m × 2 m, along the $x$-, $y$- and $z$-directions, respectively, with a discretization of $\Delta x \times \Delta y \times \Delta z = 0.1$ m × 0.1 m × 0.02 m, yielding $3 \times 10^6$ elements. The corresponding log-hydraulic conductivity field is shown in Figure 3A1.

As specified in section 2, in cases 1 and 3, periodic boundary conditions are applied for hydraulic head in all directions. A mean hydraulic gradient of 0.01 is applied to each realization, if applicable, in such a way that the resulting volume-averaged velocity is strictly oriented into the $x$-direction. The velocity field of case 2 is obtained by averaging all velocity components of 50 realizations along the $x$-direction. Figure 3B1 shows the $y$- and $z$-components of the resulting two-dimensional velocity field, which is overlain by the primary motion in the $x$-direction. Arrows indicate the direction and absolute value of the velocity, while color contour lines indicate continuous advective paths in the secondary velocity field. The nonstationary spatial anisotropy of the locally isotropic conductivity field causes significant secondary motion. In case 1, both the primary and secondary motions are perturbed by small-scale variation in the $x$-direction, whereas the upscaled velocity field of case 2 agrees well with the analytical results of *Hemker and Bakker* [2006], who analyzed groundwater whirls in piecewise uniform anisotropic hydraulic conductivity fields.

The log-hydraulic conductivity field of case 3 shares with case 1 the same mean, variance, and volume-averaged covariance function, but it is composed of a single stationary block obtained by generating a new stationary log conductivity field with the same power spectrum of the composed field used in the case 1. As can be seen in Figure 3A2, the resulting log conductivity field shows cross-like structures of high- and low-conductivity values. Figure 3B2 shows the resulting mean transverse velocity field, obtained by averaging 50 realizations of the velocity field of case 3 along the $x$-direction. The streamlines are represented using the same color scale as used in Figure 3B1. As expected, only spurious secondary motion of small spatial extent can be

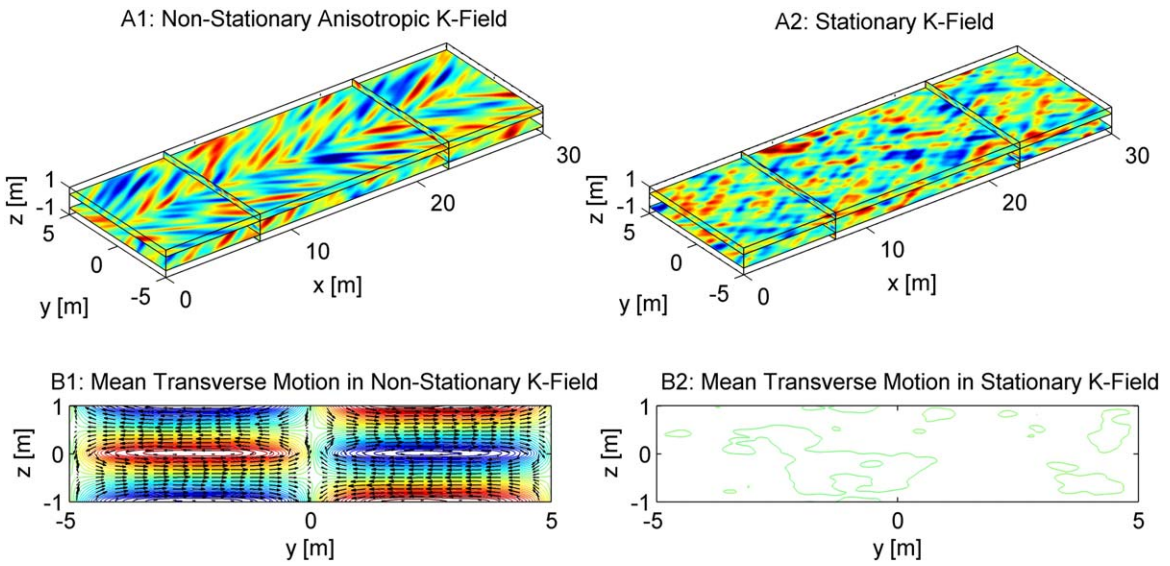


**Figure 3.** Illustration of the test cases considered. (a) Log-hydraulic conductivity fields; (b) transverse velocity fields averaged over the direction of mean flow *x*.

identified. If the unit cell was extended over a larger length in the *x*-direction, or if the number of realizations was significantly been increased, the secondary motion of the stationary field would completely disappear.

Based on the four periodic velocity fields, we constructed 50,000 streamlines using starting points on a regular grid of $\Delta y \times \Delta z = 0.02\,\text{m} \times 0.02\,\text{m}$ covering the entire inlet face of the unit cell at $x = 0$ m. Observation planes were constructed at distances of 0.1 m in the *x*-direction. The streamlines were tracked over a distance of 60 m in the *x*-direction. Because of the periodic boundary conditions and the periodic *K*-field, the velocity field is infinitely self-repetitive in all directions and streamlines can be tracked through neighboring unit cells. From the streamlines of 10 realizations each, we computed the one-particle variances, $\sigma_Y^2(x)$ and $\sigma_Z^2(x)$, of advective transverse displacement as a function of travel distance and the two-particle semivariograms of advective transverse displacement, $\gamma_Y(x)$ and $\gamma_Z(x)$, according to equation (16), considering directly neighboring streamlines in the inlet face, $y_{1,0} - y_{2,0} = 0.02$ m and $z_{1,0} - z_{2,0} = 0.02$ m, respectively.

In addition, we computed the kinematic metrics of the flow field discussed by *Chiogna et al.* [2015], namely the dimensionless stretching and folding coefficients $\langle A^2(x) \rangle$ and $\langle D^2(x) \rangle$, which quantify the affine (linear) and nonaffine (nonlinear) contributions to the deformation of a plume cross section by advection, respectively, in which the initial cross section is a small circle with radius 0.04 m [*Kelley and Ouellette*, 2011].

For steady-state advective-dispersive transport, we make use of periodicity in a slightly different way. Considering the periodicity of the boundary conditions, a source zone with dimensions $2\,\text{m} \times 0.4\,\text{m}$ was placed at the center of the inlet face of each unit cell. Outside the source, the concentration within the inlet face was set to zero. Because of periodicity, a streamline laterally leaving the unit cell to a neighboring cell is replaced by a streamline entering on the opposite face with identical concentration. Thus, it is sufficient to simulate a single thread of unit cells aligned in the *x*-direction with a constant number of streamlines within the cross sections.

The parameters used in the transport calculations are a porosity of 0.4, a pore diffusion coefficient $D_p$ of $1 \times 10^{-9}\,\text{m}^2/\text{s}$, and a transverse dispersivity $\alpha_t$ of $1 \times 10^{-3}$m. Steady-state advective-dispersive transport was simulated only for a single realization each of cases 1 and 3. From the concentration distributions within the observation planes, we computed the flux-related dilution indices $E_Q(x)$ by equations (17) and (18) and scaled them by the total discharge $Q_{tot}$ passing through a unit cell in the *x*-direction, which is the upper limit $E_Q^{\max}$ of the dilution index in the given setting. The ratio $E_Q(x)/E_Q^{\max}$ is denoted reactor ratio [*Kitanidis*, 1994; *Rolle et al.*, 2009; *Chiogna et al.*, 2011b]. The quicker $E_Q(x)/E_Q^{\max}$ approaches unity, the stronger is transverse mixing within the domain.

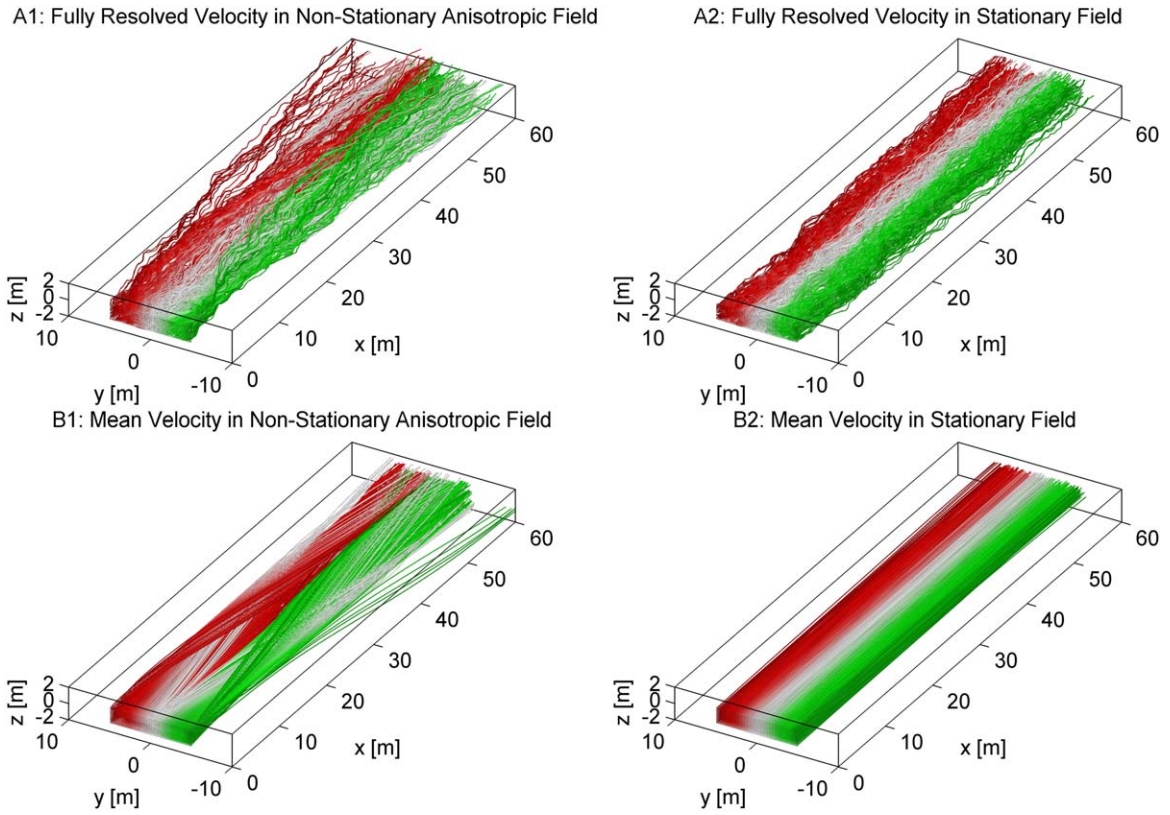


**Figure 4.** Selected streamlines of the four test cases. Color coding refers to the *y*-coordinate in the inlet face.

## 5. Results

### 5.1. Flow Fields

Figure 4 visualizes the velocity fields of the four cases described above by selected streamlines starting on a regular grid at the inlet face of a unit cell. While the top two figures show results for single realizations of the fully resolved velocity fields (cases 1 and 3), the bottom two figures show streamlines for ensemble-averaged velocity fields averaged over the *x*-coordinate (cases 2 and 4). The secondary motion of the non-stationary anisotropic *K*-field shown on Figure 3b1 leads to whirling motion in the longitudinally averaged velocity field (case 2) shown in Figure 4B1. Small-scale fluctuations are superimposed to this motion in the fully resolved velocity field for the nonstationary anisotropic *K*-field shown on Figure 4A1 (case 1). However, the secondary motion is still visible when tracking individual streamlines.

When the equivalent stationary *K*-field is used, the resulting flow field does not show persistent secondary motion, as can be seen by inspection of Figure 3B2. This behavior is also expected from theory because any stationary covariance function of log conductivity in conjunction with a uniform-in-the-average hydraulic gradients results in a uniform expected value of the velocity vector. As a consequence, the streamlines for the longitudinally averaged velocity field (case 4) shown in Figure 4B2 exhibit only spurious twists, which may be considered artifacts of a longitudinal averaging size that was not large enough to obtain operational ergodicity and a too small ensemble size of 50 realizations. Like in the nonstationary case, the streamlines for the fully resolved equivalent stationary velocity field (case 2, Figure 4A2) exhibit small-scale fluctuations about the general trend.

Table 1 summarizes standard statistics of the specific-discharge components for the four velocity fields. The different correlation structures of the log-hydraulic conductivity field lead to a 2.5% smaller mean longitudinal velocity in the stationary case in comparison to the nonstationary anisotropic case when applying the same hydraulic gradient. This rather small difference cannot explain the extent of differences in mixing

**Table 1.** Statistical Characteristics of the Velocity Fields in the Four Test Cases[a]

| Case | $\mu_{q_x}$ (m/s) | $\sigma_{q_x}/\mu_{q_x}$ | $\sigma_{q_y}/\mu_{q_x}$ | $\sigma_{q_z}/\mu_{q_x}$ |
|---|---|---|---|---|
| 1 | $2.03\times10^{-6}$ | 1.691 | 0.627 | 0.180 |
| 2 | $2.03\times10^{-6}$ | 0.120 | 0.133 | 0.029 |
| 3 | $1.98\times10^{-6}$ | 1.549 | 0.438 | 0.208 |
| 4 | $1.98\times10^{-6}$ | 0.047 | 0.007 | 0.003 |

[a] $\mu_{q_x}$: mean specific-discharge component in main direction of flow and $\sigma_{q_i}$: standard deviation of specific-discharge component in direction *i*.

discussed below. The variability within the *x*-direction of the three specific-discharge components is substantial in the fully resolved cases, which becomes obvious when comparing the normalized standard deviations of case 1 to that of case 2, and of case 3 to that of case 4, respectively. The variability of the horizontal transverse specific-discharge component $q_y$ is bigger for the nonstationary case than for the equivalent stationary one, but the difference with the respective averaged velocity fields is moderate (compare case 1 with case 3 in Table 1). The vertical velocity component varies slightly more in the stationary case 3 than in the companion nonstationary case 1. This may be explained by a more pronounced vertical connectivity of case 3, with respect to case 1, thereby leading to a less extended connected high-velocity features in horizontal directions.

Figure 5 shows the horizontal correlation function $\varrho_{q_y q_y}(\Delta x, \Delta y)$ of the specific-discharge component $q_y$:

$$\varrho_{q_y q_y}(\Delta x, \Delta y) = \frac{\overline{\left(q_y(x+\Delta x, y+\Delta y)-\bar{q}_y\right)\left(q_y(x,y)-\bar{q}_y\right)}}{\sigma^2_{q_y}}, \tag{22}$$

for cases 1 and 3. In equation (22), the overbar denotes the volume average over the entire unit cell and the ensemble average over 50 realizations. Fluctuations of $q_y$ show persistent high correlation in both stationary and nonstationary log conductivity fields. On the other hand, the negative correlation in the longitudinal direction is more pronounced in the stationary case in comparison to the nonstationary one. Also, the nonstationary fields hardly exhibit negative correlations of $q_y$ for separation distances on the order of half the width of the unit cell, whereas the stationary case shows alternating sectors of positive and negative correlations. In interpreting these results, however, it should be considered that the two-point correlation of $q_y$ may be somewhat misleading when applied to the analysis of a nonstationary velocity field because nonstationarity introduces variations (trends) of the mean velocity field in the transverse directions, as illustrated in Figure 3B1, which is not accounted for in equation (22).

### 5.2. Second Moments of Transverse Displacements in Advective Transport

Figure 6 shows the second-order statistical metrics of the transverse displacements, $\sigma^2_Y(x), \sigma^2_Z(x), \gamma_Y(x)$, and $\gamma_Z(x)$, as a function of the travel distance in the *x*-direction for the four cases considered in the present work.

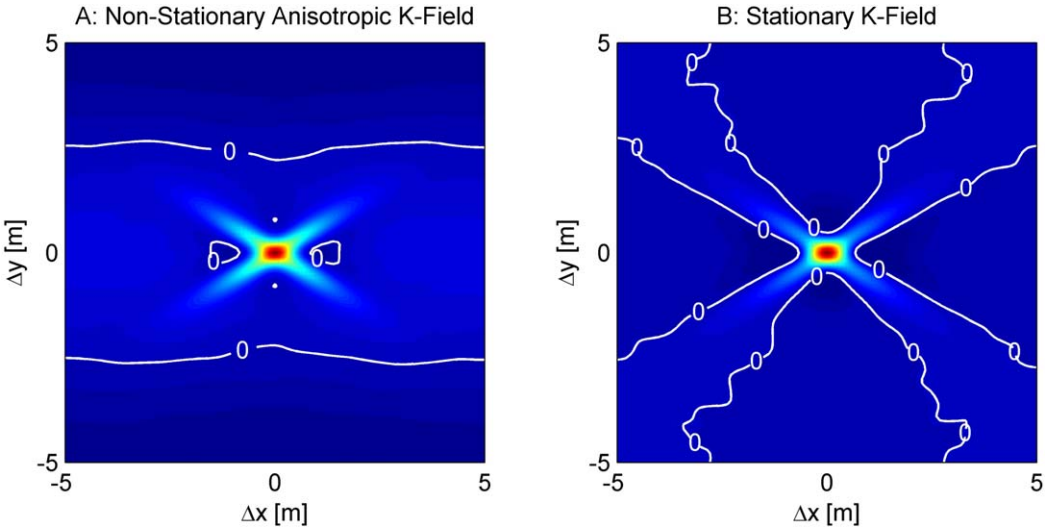


**Figure 5.** Horizontal correlation function $\varrho_{q_y q_y}(\Delta x, \Delta y)$ of the horizontal transverse specific-discharge component $q_y$. (a) For the nonstationary anisotropic *K*-field as shown in Figure 3A1; (b) for the equivalent stationary *K*-field as shown in Figure 3A2. The dark red color at the origin refers to a correlation coefficient of one, whereas dark blue colors indicate negative correlation coefficients.

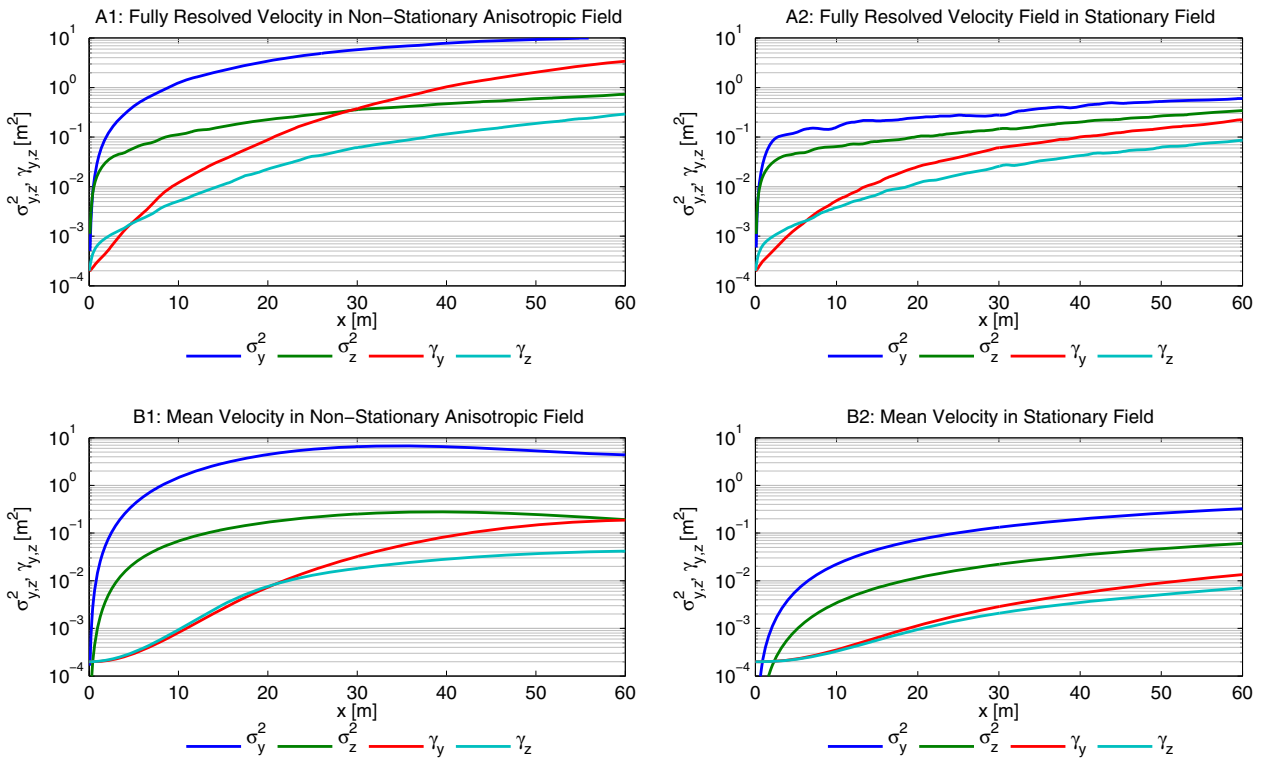


**Figure 6.** Numerical moments of advective transverse displacement as function of travel distance in the four test cases. $\sigma^2_Y$: one-particle variance of horizontal transverse displacement; $\sigma^2_Z$: one-particle variance of vertical transverse displacement; $\gamma_Y$: two-particle semivariogram of horizontal transverse displacement for an initial distance $\Delta y_0 = 0.02$ m; and $\gamma_Z$: two-particle semivariogram of vertical transverse displacement for an initial distance $\Delta z_0 = 0.02$ m.

To obtain the results for the fully resolved cases 1 and 3, we averaged over 10 realizations and all starting points at the inlet face. The most striking result shown in this figure is that the variance of the residual horizontal transverse displacement $\sigma^2_Y(x)$ and the corresponding semivariogram $\gamma_Y(x)$ are more than a factor of 10 larger for the nonstationary anisotropic case 1 than for the equivalent stationary case 3. This is so even though the correlation structures shown in Figure 5 are similar and the velocity variances $\sigma^2_{q_y}$, listed in Table 1, differ only by a factor of $\approx 1.43$. We explain the differences in $\sigma^2_Y(x)$ and $\gamma_Y(x)$ by the deterministic persistence of transverse-velocity fluctuations in the nonstationary anisotropic field, which is not quantified by the metrics $\sigma^2_{q_y}$ and $\varrho_{q_y q_y}(\Delta x, \Delta y)$ used in first-order stochastic theory of ensemble and effective dispersion. A major consequence of $\gamma_Y(x)$ being bigger in case 1 than in case 3 is that solutes that are transferred by transverse dispersion (not considered here) from one streamline to its neighboring streamline are carried away by advection in a substantially different direction when this happens in a flow field with mean secondary motion, rather than in a stationary velocity field, for which neighboring streamlines tend to stick together due to the absence of a secondary mean motion. This effect can be observed also for the metrics of vertical displacement, $\sigma^2_Z(x)$ and $\gamma_Z(x)$, but is by far not as pronounced as in the horizontal direction.

For the first 30 m, the variance of horizontal transverse displacements $\sigma^2_Y(x)$ is similar but not identical for cases 1 and 2, that is, the nonstationary field with resolved 3-D velocity field and with $x$-averaged velocity, respectively (Figures 6A1 and 6B1). The extended secondary motion plays a major role for $\sigma^2_Y(x)$; about half the particles move to the right and the other half to the left. These particles consistently return to the middle in averaged flow field of case 2, causing $\sigma^2_Y(x)$ to decrease for $x > 30$m, whereas no such behavior is observed in the fully resolved case 1. In case 2, neighboring streamlines stay close together, as can be argued from the fact that the semivariogram $\gamma_Y(x)$ of horizontal transverse displacement is much smaller than $\sigma^2_Y$. This indicates that the plume may be separated, by secondary motion, but the resulting parts remain compact if small-velocity fluctuations are neglected. Considering now the equivalent stationary flow fields of cases 3 and 4, it can be observed that $\sigma^2_Y(x)$ and $\gamma_Y(x)$ are smaller for the averaged velocity field 4 than in the fully resolved case 3. The metrics of vertical displacements are smaller than the horizontal counterparts in all cases.

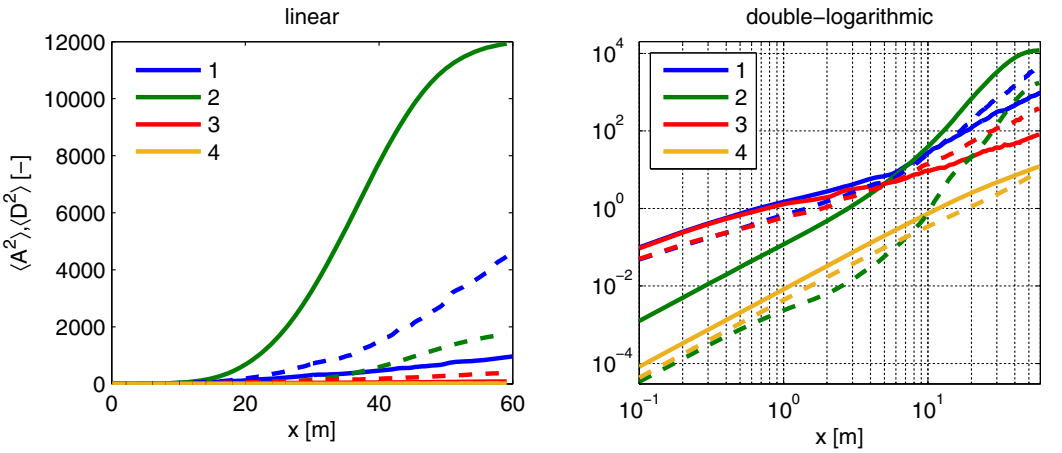


**Figure 7.** Stretching (solid lines) and folding (dashed lines) metrics $\langle A^2(x)\rangle$ and $\langle D^2(x)\rangle$ for the four test cases as a function of distance $x$ from the inlet plane. (left) Double linear scale; (right) double logarithmic scale. Blue lines: fully resolved velocity field 1 with nonstationary anisotropy; green lines: length- and ensemble-averaged velocity field 2 for nonstationary anisotropy; red lines: fully resolved velocity field 3 with equivalent stationary correlation function of ln $K$; and orange lines: length- and ensemble-averaged velocity field 4 for the stationary case.

### 5.3. Stretching and Folding in Advective Transport

Figure 7 shows the dimensionless metrics of advective stretching, $\langle A^2(x)\rangle$, and folding, $\langle D^2(x)\rangle$ for the four test cases as a function of distance. $\langle A^2(x)\rangle$ quantifies the linear contribution of the deformation of the plume cross-section from the inlet plane to the plane at $x$, whereas $\langle D^2(x)\rangle$ quantifies the nonlinear contribution (for discussion see *Chiogna et al.*, 2015). At distances of up to $\approx$ 5m, the small-scale velocity variations of the fully resolved fields 1 and 3 dominate stretching and folding to a very similar extent. This distance is on the order of the correlation length $I_1$ of 4 m. At larger distances, the nonstationary case 1 and the stationary case 3 strongly deviate with both stretching and folding of the nonstationary case being larger by about one order of magnitude.

At larger distances, stretching is the biggest for the averaged nonstationary case 2. Folding of this case is initially very small in comparison to the fully resolved fields 1 and 3. However, from distances of about 30 m on, folding is stronger in case 2 than in case 3. This behavior indicates very regular and strong advective deformation of the plume cross-section over a significant distance, but at larger distances the deformation contains a significant nonlinear contribution that is associated folding.

In theory, both advective stretching and folding of the averaged stationary velocity field 4 should be zero, because the perfect average would be a uniform velocity distribution. The small remaining values of $\langle A^2(x)\rangle$ and $\langle D^2(x)\rangle$ for this case, presented in Figure 7, reflect spurious velocity fluctuations caused by a too small ensemble size of 50 and a too small averaging length.

### 5.4. Steady-State Concentrations in Advective-Dispersive Transport

The results discussed so far are for strictly advective transport, i.e., in the absence of local dispersion. The effect of local dispersion is explored in Figure 8 which shows the steady-state concentration distributions at observation planes along the longitudinal direction $x$ and in the presence of local dispersion. The concentration distributions shown in this figure were obtained using the scheme discussed in section 3, which is free of artificial (numerical) transverse dispersion, typically introduced by Eulerian approximations of the advective term in the transport equation, equation (11) on grids that are not aligned with streamlines [*Cirpka et al.*, 1999c]. The columns show concentration profiles at the control planes indicated on the left of the figure for cases from 1 to 4. In particular, column 1 is for the fully resolved velocity field obtained with the nonstationary log conductivity field generated as described in section 4, while column 2 is for the smoothed velocity field obtained by averaging the ensemble-averaged velocity of case 1 along the $x$-direction. Columns 3 and 4 refer to the fully resolved and averaged stationary log conductivity fields, respectively. The supporting information contains two movies

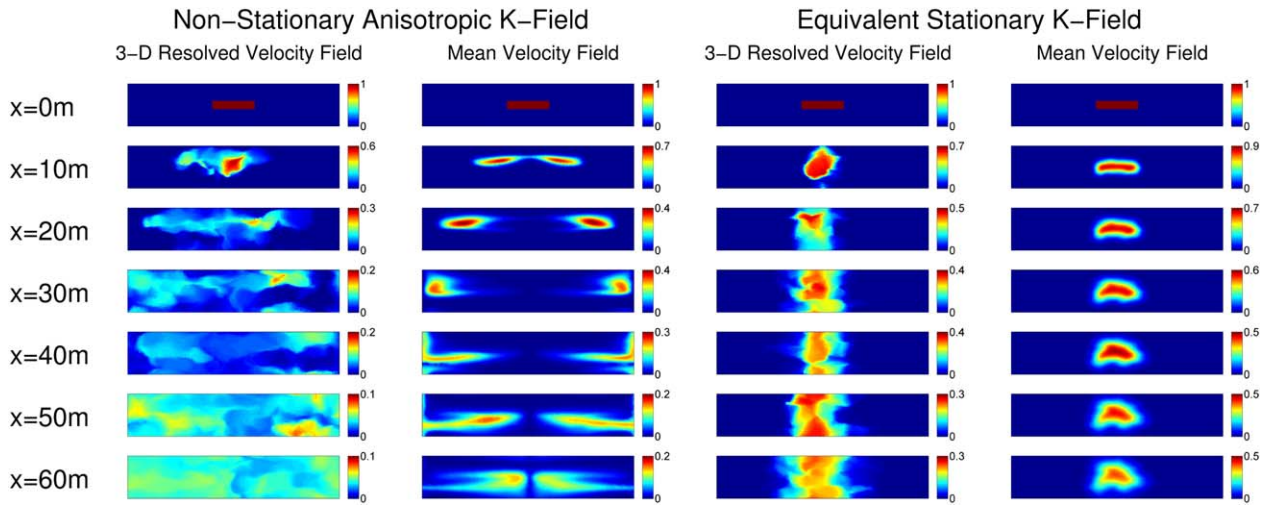


**Figure 8.** Steady state concentration distributions in observation planes perpendicular to the mean flow direction for all four test cases. Concentrations are normalized by the concentration of the source. Spatial dimensions of the cross sections: 10 m × 4 m. Color axes differ from plot to plot.

visualizing the steady-state concentration distributions of the fully resolved nonstationary and stationary cases. Here the concentration distribution within a moving plane perpendicular to the main flow direction $x$ is shown, giving more insight in the evolution of the plumes with $x$ than the individual planes presented in Figure 8.

The concentration fields depicted in column 1 show that the secondary motion caused by nonstationarity in the log conductivity field results in more effective transverse spreading and in lower peak concentrations in comparison to the equivalent stationary case (column 3). The plume initially splits into two parts, because the source zone is at a divergence point of the secondary motion, but clear plume fractions are difficult to identify. Over the travel distance of 60 m, the periodic concentration field almost approaches the asymptotic uniform normalized concentration distribution of 0.04.

The splitting of the plume into two parts is more evident in case 2, where the velocity field of the nonstationary case 1 is averaged along the $x$-direction and over 50 realizations, obtaining a transverse secondary motion not overlain by small-scale fluctuations. The two portions in which the plume is split remain separated as they move downstream, although mass exchange by transverse dispersion results in the increase of the volume occupied by the solute. The effect is less pronounced than in case 1, but stronger than in the stationary fields (cases 3 and 4). This is caused by nonuniformity in the rotational velocity of secondary motion, which enhances stretching of the interface between the plume and the surrounding ambient solution, thereby leading to large transverse solute transport with respect to the cases 3 and 4.

The steady-state concentration fields for advective-dispersive transport in the equivalent stationary log-hydraulic conductivity field are quite different: In the 3-D resolved velocity field, the plume does not spread intensively in the horizontal lateral direction, whereas vertical dilution is more pronounced, which is in accordance with the enlarged variance $\sigma^2_{q_z}$ of the vertical specific-discharge component. The ensemble- and $x$-averaged velocity field of case 4 is so uniform that the plume is hardly deformed.

### 5.5. Plume Dilution

To quantify dilution, we have computed the flux-related reactor ratio $E_Q/E_Q^{\max}$ for all cross sections according to equation (17), considering that $E_Q^{\max}$ equals the total discharge passing through the unit cell. The calculated values of $E_Q(x)/E_Q^{\max}$ are plotted as black lines in Figure 9 as a function of travel distance $x$. For comparison, we also computed the reactor ratio of the concentration distribution $c_{\text{hom}}$ $[M\,L^3]$ for a rectangular source in a periodic uniform flow field with uniform seepage velocity $v = 5\times10^{-6}$m/s and various isotropic transverse dispersion coefficients $D_t$:

$$\frac{c_{\mathrm{hom}}(x,y,z)}{c_s} = \sum_{j=-\infty}^{+\infty}\sum_{k=-\infty}^{+\infty}\frac{1}{4}\left(\mathrm{erf}\left(\frac{y+\frac{w}{2}+jW}{2\sqrt{\frac{D_t x}{v}}}\right)-\mathrm{erf}\left(\frac{y-\frac{w}{2}+jW}{2\sqrt{\frac{D_t x}{v}}}\right)\right)\times \left(\mathrm{erf}\left(\frac{z+\frac{h}{2}+kH}{2\sqrt{\frac{D_t x}{v}}}\right)-\mathrm{erf}\left(\frac{z-\frac{h}{2}+kH}{2\sqrt{\frac{D_t x}{v}}}\right)\right), \tag{23}$$

in which $c_s$ [$M\,L^3$] is the solute concentration within the source, which is $w = 2$ m wide and $h = 0.4$ m high, whereas the unit cell is $W = 10$ m wide and $H = 2$ m high. The infinite sums in equation (23) arise from periodicity in the $y$- and $z$-directions. On the validity of equation (23) and its underlying assumptions, refer to *Srinivasan et al.* [2007]. The resulting reactor ratios are plotted in the background of Figure 9 as a function of travel distance $x$ and $D_t$, where the color indicates the $\log_{10}(D_t)$-value. In the following, we denote the value of transverse-dispersion coefficient that would be needed in a homogeneous flow field to meet the same reactor ratio as in the heterogeneous test cases the equivalent transverse dispersion coefficient $D_t^{eq}$ [$L^2\,T^{-1}$].

Figure 9 clearly shows that the nonstationary anisotropic variability of log-hydraulic conductivity leads to a significant enhancement of dilution. After 60 m of travel distance, the dilution of case 1 is almost complete. In a homogeneous flow field with identical pore diffusion coefficient, mean seepage velocity, and transverse dispersivity, the transverse dispersion coefficient $D_t$ would be $6\times10^{-9}\mathrm{m}^2/\mathrm{s}$. In comparison to that, the degree of dilution reached after 60 m travel distance is in case 1 equivalent to an increase of $D_t$ in the homogeneous flow field by a factor of 77 ($D_t^{eq} \approx 4.7\times10^{-7}\mathrm{m}^2/\mathrm{s}$). As can be seen from Figure 9, the mixing enhancement in this case is a continuous process, that has not reached Fickian scaling at the end of the considered domain, that is, the equivalent transverse dispersion coefficient of a homogeneous domain causing the same amount of dilution, still increases.

Quite interestingly, the averaged velocity field of case 2, which shows the clearest secondary motion, ranks second in the degree of dilution reached (which is equivalent to a homogeneous case with $D_t^{eq} \approx 9.4\times10^{-8}\mathrm{m}^2/\mathrm{s}$). The secondary motion brings solute-loaded streamlines constantly into contact with hardly loaded streamlines, at least over the travel distance considered. While small-scale fluctuations and associated flow focusing are an important addition to mixing enhancement in case 1, the effect of secondary motion appears to be more important. This becomes evident when considering dilution caused by the stationary, 3-D resolved velocity field of case 3. In contrast to the previous two cases, the scaling of the flux-related reactor ratio with travel distance here approaches a behavior similar to Fickian transverse dispersion in uniform flow. Expressed in terms of an equivalent transverse dispersion coefficient, $D_t^{eq} \approx 2.1\times10^{-8}\mathrm{m}^2/\mathrm{s}$, which relates to an increase of $D_t$ by about a factor of 3.5, which is in the order of magnitude of the enhancement factors by flow focusing in two-dimensional domains reported by *Cirpka et al.* [2011].

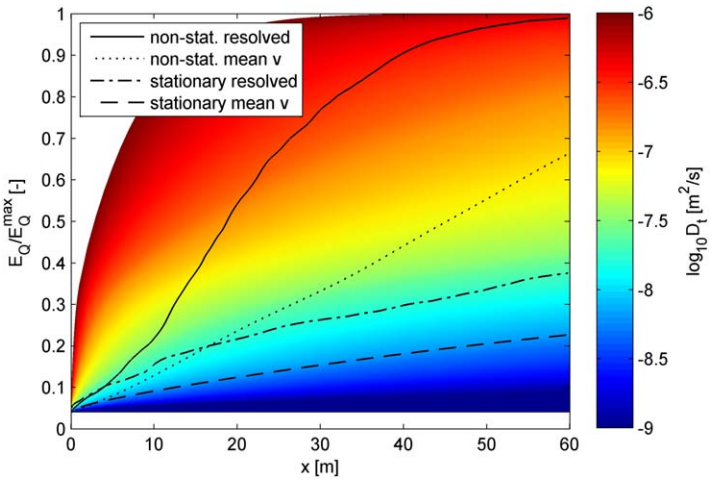


**Figure 9.** Flux-related reactor ratio $E_Q/E_Q^{\max}$ as a function of travel distance for advective-dispersive transport in the four test cases. Solid line: fully resolved velocity in nonstationary anisotropic field; dotted line: mean velocity in nonstationary anisotropic field; dash-dotted line: fully resolved velocity in stationary field; and dashed line: mean velocity in stationary field. Color plot in the background: reactor ratio as a function of distance for a homogeneous velocity field ($v=5\times10^{-6}\mathrm{m}/\mathrm{s}$) for various isotropic transverse dispersion coefficients.

It is interesting to see that the order of dilution intensity among the test cases is identical to the order of the folding metric $\langle D^2(x)\rangle$ shown in Figure 7. Even the transition

point at which dilution becomes larger in case 2 than in case 3 is comparable. By contrast, the stretching metric $\langle A^2(x)\rangle$ is not a good indicator of mixing.

## 6. Discussion and Conclusions

The present study has shown that nonstationary anisotropy of hydraulic conductivity can have a significant impact on transverse mixing in steady-state groundwater flow. While nonstationary anisotropy of hydraulic conductivity has not been studied very intensively in the past, we are convinced that it is common in natural sedimentary deposits, which are characterized by a hierarchy of internally anisotropic structural elements of limited spatial extent. The orientation of anisotropy typically differs from one structural element to the other, thus leading to anisotropy in hydraulic conductivity that is stationary only within individual structural units. In most practical applications, it is very difficult to detect the exact sedimentary structure. While individual drilling logs indicate "layering" of the sediments, the lateral extent of the units and the orientation of anisotropy is often missing. Thus, while common sedimentological knowledge and outcrop analogs [e.g., *Heinz et al*., 2003; *Bayer et al*., 2011] make us believe that nonstationary anisotropy is rather the rule than the exception, it is difficult to measure within a specific aquifer. This makes it even more important to study what is missing when we blend out this structural feature of aquifers.

In the present study, we have simplified the complexity of real sediments by considering blocks of heterogeneous log conductivity with anisotropic correlation functions differing in their spatial orientation. The nonstationary anisotropy of heterogeneity caused mean secondary motion of groundwater flow resulting in enhanced transverse mixing of a solute plume. The secondary motion makes the trajectories of solute particles, which start at the same location and are initially separated by pore-scale dispersion, diverge at a rate that is much bigger than by Fickian dispersion only. In previous two-dimensional studies, where enhancement of transverse mixing was restricted to flow-focusing effects [*Bauer et al*., 2009b; *Cirpka et al*., 2011; *Werth et al*., 2006], heterogeneity only led to a moderate increase of equivalent transverse dispersion coefficients in comparison to the homogeneous case. The flow topology caused by nonstationary three-dimensional anisotropy analyzed here, by contrast, led to a remarkably larger increase. These findings are in agreement with the observation of *Maier and Grathwohl* [2006], suggesting that mixing-controlled steady-state plumes at the field scale are significantly shorter than predicted applying local-scale transverse dispersion coefficients derived in laboratory setups. This study, for the first time, provides a potential mechanistic explanation of this observation.

Among the topological and kinematic descriptors of the flow field discussed in *Chiogna et al.* [2015], the folding metric $\langle D^2(x)\rangle$ has the highest predictive power with respect to mixing, whereas the stretching metric $\langle A^2(x)\rangle$ is much less informative. The local helicity density, discussed also by *Chiogna et al.* [2015], may be misleading as it describes larger-scale twisting only when the flow field is properly upscaled. Because hydraulic conductivity is locally isotropic, the helicity density is locally zero in the fully resolved nonstationary test case 1, but mixing is the strongest. *Chiogna et al.* [2015] argue that topological metrics for the study of mixing processes should be applied to velocity fields at the appropriate scale of interest. A similar conclusion was reached by *de Barros et al*. [2012] for the Okubo-Weiss parameter in case of stationary two-dimensional flows in heterogeneous porous media.

It may be worth noting that different definitions of stretching and folding exist. For example, *Le Borgne et al*. [2013] analyzed the elongation of plume lamella in transient transport through heterogeneous porous media. The latter authors analyzed how dispersive mass transfer perpendicular to the lamella contributes to plume dilution, quantified by the scalar dissipation rate. Transverse mixing, however, also makes the lamella coalesce. The setting in the present study is slightly different, as we analyze transverse mixing in steady-state transport. However, changing time with longitudinal distance, our plumes look like undergoing transient stirring in two-dimensional rotational flows, potentially facilitating an analysis similar to that of *Le Borgne et al*. [2013].

The purpose of the present study was to describe the phenomenon of enhanced transverse mixing by groundwater whirls caused by nonstationary anisotropy of hydraulic conductivity. Our findings offer interesting possibilities for future investigation and might open a new field of research on solute transport in heterogeneous porous media beyond stochastic subsurface theory applied to second-order stationary fields. In particular, it will become necessary to develop upscaling rules that relate structural properties of

the (log)-hydraulic conductivity field, such as the dimensions of typical sedimentary elements and the variation the internal anisotropy, to topological and kinematic properties of the flow field, such as the variance and correlation structure of $\nabla \times \mathbf{q}$ or the folding metric $\langle D^2(x) \rangle$, and finally effective transverse mixing coefficients. Existing approaches to characterize hierarchical sedimentary structure, such as those of *Scheibe and Freyberg* [1995] and [*Ritzi et al*., 2004], may be good starting points. However, traditional analyses of these fields by constructing stationary covariance functions and deriving macrodispersion coefficients [*Ritzi et al*., 2004; *Dai et al*., 2004] have overlooked the importance of nonstationary anisotropy so far.

Previous studies have shown that local transverse dispersion depends on molecular diffusion even at high velocities [*Chiogna et al*., 2010]. In two-dimensional simulations, the compound-specific effects of transverse mixing did not vanish in heterogeneous domains [*Chiogna et al*., 2011a; *Cirpka et al*., 2011]. In the present study, we have restricted the analysis to the standard linear model of $D_t$ according to *Scheidegger* [1961] for the ease of computation. We believe that compound-specific effects will also prevail in the current setting of nonstationary anisotropic log conductivity fields over large travel distances as local-scale transverse dispersion controls the transition from plume deformation to actual mixing. At very large distances, when mixing has caught up with plume deformation, compound-specific effects may vanish, but it is unlikely that this regime is reached in realistic scenarios.

**Acknowledgments**
This work has been supported by Deutsche Forschungsgemeinschaft under the grants Ci 26/11-1 and Ro 4169/3-1. M.R. acknowledges the support of the Marie Curie International Outgoing Fellowship (DILREACT project) within the 7th European Community Framework Programme. A.B. acknowledges the funding by the Italian Ministry of Education, Universities and Research through the project Innovative Methods for Water Resources Management Under Hydro-Climatic Uncertainty Scenarios (2010JHF437).

## References

Acharya, R. C., A. J. Valocchi, C. J. Werth, and T. W. Willingham (2007), Pore-scale simulation of dispersion and reaction along a transverse mixing zone in two-dimensional porous media, *Water Resour. Res.*, *43*, W10435, doi:10.1029/2007WR005969.

Andricevic, R., and V. Cvetkovic (1998), Relative dispersion for solute flux in aquifers, *J. Fluid Mech.*, *361*, 145–174.

Anneser, B., F. Einsiedl, R. U. Meckenstock, L. Richters, F. Wisotzky, and C. Griebler (2008), High-resolution monitoring of biogeochemical gradients in a tar oil-contaminated aquifer, *Appl. Geochem.*, *23*(6), 1715–1730, doi:10.1016/j.apgeochem.2008.02.003.

Attinger, S., M. Dentz, and W. Kinzelbach (2004), Exact transverse macro dispersion coefficients for transport in heterogeneous porous media, *Stochastic Environ. Res. Risk Assess.*, *18*(1), 9–15.

Bakker, M., and K. Hemker (2004), Analytic solutions for groundwater whirls in box-shaped, layered anisotropic aquifers, *Adv. Water Res.*, *27*(11), 1075–1086.

Bauer, R. D., M. Rolle, P. Kuerzinger, P. Grathwohl, R. U. Meckenstock, and C. Griebler (2009a), Two-dimensional flow-through microcosms—Versatile test systems to study biodegradation processes in porous aquifers, *J. Hydrol.*, *369*(3–4), 284–295, doi:10.1016/j.jhydrol.2009.02.037.

Bauer, R. D., M. Rolle, S. Bauer, C. Eberhardt, P. Grathwohl, O. Kolditz, R. U. Meckenstock, and C. Griebler (2009b), Enhanced biodegradation by hydraulic heterogeneities in petroleum hydrocarbon plumes, *J. Contam. Hydrol.*, *105*(1–2), 56–68, doi:10.1016/j.jconhyd.2008.11.004.

Bayer, P., P. Huggenberger, P. Renard, and A. Comunian (2011), Three-dimensional high resolution fluvio-glacial aquifer analog: Part 1: Field study, *J. Hydrol.*, *405*(1–2), 1–9, doi:10.1016/j.jhydrol.2011.03.038.

Bear, J. (1972), *Dynamics of Fluids in Porous Media*, Elsevier, N. Y.

Bellin, A., and D. Tonina (2007), Probability density function of non-reactive solute concentration in heterogeneous porous formations, *J. Contam. Hydrol.*, *94*(1–2), 109–125.

Boso, F., A. Bellin, and M. Dumbser (2013), Numerical simulations of solute transport in highly heterogeneous formations: A comparison of alternative numerical schemes, *Adv. Water Resour.*, *52*, 178–189, doi:10.1016/j.advwatres.2012.08.006.

Carle, S. F., and G. E. Fogg (1997), Modeling spatial variability with one and multidimensional continuous-lag Markov chains, *Math. Geol.*, *29*(7), 891–918.

Caroni, E., and V. Fiorotto (2005), Analysis of concentration as sampled in natural aquifers, *Transp. Porous Media*, *59*(1), 19–45.

Chiogna, C., O. A. Cirpka, P. Grathwohl, and M. Rolle (2011a), Relevance of local compound-specific transverse dispersion for conservative and reactive mixing in heterogeneous porous media, *Water Resour. Res.*, *47*, W07540, doi:10.1029/2010WR010270.

Chiogna, G., C. Eberhardt, P. Grathwohl, O. A. Cirpka, and M. Rolle (2010), Evidence of compound dependent hydrodynamic and (hydro)-mechanical transverse dispersion by multi-tracer laboratory experiments, *Environ. Sci. Technol.*, *44*(2), 688–693, doi:10.1021/es9023964.

Chiogna, G., O. A. Cirpka, P. Grathwohl, and M. Rolle (2011b), Transverse mixing of conservative and reactive tracers in porous media: Quantification through the concepts of flux-related and critical dilution indices, *Water Resour. Res.*, *47*, W02505, doi:10.1029/2010WR009608.

Chiogna, G., D. L. Hochstetter, A. Bellin, P. K. Kitanidis, and M. Rolle (2012), Mixing, entropy and reactive solute transport, *Geophys. Res. Lett.*, *39*, L20405, doi:10.1029/2012GL053295.

Chiogna, G., O. A. Cirpka, M. Rolle, and A. Bellin (2015), Helical flow in three-dimensional nonstationary anisotropic heterogeneous porous media, *Water Resour. Res.*, *51*, doi:10.1002/2014WR015330.

Cirpka, O., M. Rolle, G. Chiogna, F. P. J. de Barros, and W. Nowack (2012), Stochastic evaluation of mixing-controlled steady-state plume lengths in two-dimensional heterogeneous domains, *J. Contam. Hydrol.*, *138–139*, 22–39.

Cirpka, O. A., and P. K. Kitanidis (2000), Characterization of mixing and dilution in heterogeneous aquifers by means of local temporal moments, *Water Resour. Res.*, *36*(5), 1221–1236.

Cirpka, O. A., and A. J. Valocchi (2007), Two-dimensional concentration distribution for mixing-controlled bioreactive transport in steady state, *Adv. Water Resour.*, *30*(6–7), 1668–1679, doi:10.1016/j.advwatres.2006.05.022.

Cirpka, O. A., and A. J. Valocchi (2009), Reply to comments on "Two-dimensional concentration distribution for mixing-controlled bioreactive transport in steady state" by H. Shao et al., *Adv. Water Resour.*, *32*(2), 298–301, doi:10.1016/j.advwatres.2008.10.018.

Cirpka, O. A., E. O. Frind, and R. Helmig (1999a), Numerical simulation of biodegradation controlled by transverse mixing, *J. Contam. Hydrol.*, *40*(2), 159–182.

Cirpka, O. A., E. O. Frind, and R. Helmig (1999b), Streamline-oriented grid-generation for transport modelling in two-dimensional domains including wells, *Adv. Water Resour.*, *22*(7), 697–710.

Cirpka, O. A., R. Helmig, and E. O. Frind (1999c), Numerical methods for reactive transport on rectangular and streamline-oriented grids, *Adv. Water Resour.*, *22*(7), 711–728.
Cirpka, O. A., Å. Olsson, Q. Ju, M. A. Rahman, and P. Grathwohl (2006), Determination of transverse dispersion coefficients from reactive plume lengths, *Ground Water*, *44*(2), 212–221, doi:10.1111/j.1745-6584.2005.00124.x.
Cirpka, O. A., F. P. J. de Barros, G. Chiogna, M. Rolle, and W. Nowak (2011), Stochastic flux-related analysis of transverse mixing in two-dimensional heterogeneous porous media, *Water Resour. Res.*, *47*, W06515, doi:10.1029/2010WR010279.
Dagan, G. (1984), Solute transport in heterogeneous porous formations, *J. Fluid Mech.*, *145*, 151–177.
Dagan, G. (1989), *Flow and Transport in Porous Formations*, Springer, N. Y.
Dagan, G. (1991), Dispersion of a passive solute in nonergodic transport by steady velocity-fields in heterogeneous formations, *J. Fluid Mech.*, *233*, 197–210.
Dai, Z., R. W. Ritzi, C. Huang, Y. N. Rubin, and D. F. Dominic (2004), Transport in heterogeneous sediments with multimodal conductivity and hierarchical organization across scales, *J. Hydrol.*, *294*(1–3), 68–86.
Davis, G. B., C. Barber, T. Power, J. Thierrin, B. M. Patterson, J. L. Rayner, and Q. Wu (1999), The variability and intrinsic remediation of a btex plume in anaerobic sulphate-rich groundwater, *J. Contam. Hydrol.*, *36*(3–4), 265–290.
de Barros, F. P. J., and W. Nowak (2010), On the link between contaminant source release conditions and plume prediction uncertainty, *J. Contam. Hydrol.*, *116*(1–4), 24–34, doi:10.1016/j.jconhyd.2010.05.004.
de Barros, F. P. J., M. Dentz, J. Koch, and W. Nowak (2012), Flow topology and scalar mixing in spatially heterogeneous flow fields, *Geophys. Res. Lett.*, *39*, L08404, doi:10.1029/2012GL051302.
de Dreuzy, J. R., and A. Beaudoin (2013), Numerical assessment of 3-D macrodispersion in heterogeneous porous media, *Water Resour. Res.*, *49*, 2489–2496, doi:10.1002/wrcr.20206.
de Marsily, G. (1986), *Quantitative Hydrogeology: Groundwater Hydrology for Engineers*, Academic, San Diego, Calif.
Dentz, M., and J. Carrera (2003), Effective dispersion in temporally fluctuating flow through a heterogeneous medium, *Phys. Rev. E*, *68*(3), 036,310, doi:10.1103/PhysRevE.68.036310.
Dentz, M., H. Kinzelbach, S. Attinger, and W. Kinzelbach (2000a), Temporal behavior of a solute cloud in a heterogeneous porous medium: 1. Point-like injection, *Water Resour. Res.*, *36*(12), 3591–3604.
Dentz, M., H. Kinzelbach, S. Attinger, and W. Kinzelbach (2000b), Temporal behavior of a solute cloud in a heterogeneous porous medium: 2. Spatially extended injection, *Water Resour. Res.*, *36*(12), 3605–3614.
Dentz, M., T. Le Borgne, A. Englert, and B. Bijeljic (2011), Mixing, spreading and reaction in heterogeneous media: A brief review, *J. Contam. Hydrol.*, *120–121*, 1–17, doi:10.1016/j.jconhyd.2010.05.002.
Dietrich, C., and G. Newsam (1993), A fast and exact method for multidimensional Gaussian stochastic simulations, *Water Resour. Res.*, *29*(8), 2861–2869.
Fiori, A. (1996), Finite Peclet extensions of Dagan's solutions to transport in anisotropic heterogeneous formations, *Water Resour. Res.*, *32*(1), 193–198.
Fiori, A. (2001), On the influence of local dispersion in solute transport through formations with evolving scales of heterogeneity, *Water Resour. Res.*, *37*(2), 235–242.
Fiori, A., and G. Dagan (2000), Concentration fluctuations in aquifer transport: A rigorous first-order solution and applications, *J. Contam. Hydrol.*, *45*(1–2), 139–163.
Fiori, A., I. Jankovic, and G. Dagan (2011), The impact of local diffusion upon mass arrival of a passive solute in transport through three-dimensional highly heterogeneous aquifers, *Adv. Water Resour.*, *34*(12), 1563–1573.
Gelhar, L. W. (1993), *Stochastic Subsurface Hydrology*, Prentice Hall, Englewood Cliffs, N. J.
Gelhar, L. W., and C. L. Axness (1983), Three-dimensional stochastic analysis of macrodispersion in aquifers, *Water Resour. Res.*, *19*(1), 161–180.
Heinz, J., S. Kleineidam, G. Teutsch, and T. Aigner (2003), Heterogeneity patterns of quaternary glaciofluvial gravel bodies (SW-Germany): Application to hydrogeology, *Sediment. Geol.*, *158*(1–2), 1–23, doi:10.1016/S0037-0738(02)00239-7.
Hemker, K., and M. Bakker (2006), Analytical solutions for whirling groundwater flow in two-dimensional heterogeneous anisotropic aquifers, *Water Resour. Res.*, *42*, W12419, doi:10.1029/2006WR004901.
Herrera, P. A., A. J. Valocchi, and R. D. Beckie (2010), A multidimensional streamline-based method to simulate reactive solute transport in heterogeneous porous media, *Adv. Water Resour.*, *33*(7), 711–727, doi:10.1016/j.advwatres.2010.03.001.
Hochstetler, D. L., M. Rolle, G. Chiogna, C. M. Haberer, P. Grathwohl, and P. K. Kitanidis (2013), Effects of compound-specific transverse mixing on steady-state reactive plumes: Insights from pore-scale simulations and Darcy-scale experiments, *Adv. Water Resour.*, *54*, 1–10.
Jankovic, I., D. R. Steward, R. J. Barnes, and G. Dagan (2009), Is transverse macrodispersivity in three-dimensional groundwater transport equal to zero? A counterexample, *Water Resour. Res.*, *45*, W08415, doi:10.1029/2009WR007741.
Kelley, D. H., and N. T. Ouellette (2011), Separating stretching from folding in fluid mixing, *Nat. Phys.*, *7*, 477–480.
Kitanidis, P., and P. McCarty (2012), *Delivery and Mixing in the Subsurface: Processes and Design Principles for In Situ Remediation, SERDP ESTCP Remediation Technol. Monogr. Ser.*, Springer, N. Y.
Kitanidis, P. K. (1988), Prediction by the method of moments of transport in heterogeneous formations, *J. Hydrol.*, *102*(1–4), 453–473.
Kitanidis, P. K. (1992), Analysis of macrodispersion through volume-averaging: Moment equations, *Stochastic Hydrol. Hydraul.*, *6*, 5–25.
Kitanidis, P. K. (1994), The concept of the dilution index, *Water Resour. Res.*, *30*(7), 2011–2026.
Le Borgne, T., M. Dentz, and E. Villermaux (2013), Stretching, coalescence, and mixing in porous media, *Phys. Rev. Lett.*, *110*(20), 204,501, doi:10.1103/PhysRevLett.110.204501.
Liedl, R., A. J. Valocchi, P. Dietrich, and P. Grathwohl (2005), Finiteness of steady state plumes, *Water Resour. Res.*, *31*, W12501, doi:10.1029/2005WR004000.
Liedl, R., P. K. Yadav, and P. Dietrich (2011), Length of 3-D mixing-controlled plumes for a fully penetrating contaminant source with finite width, *Water Resour. Res.*, *47*, W08602, doi:10.1029/2010WR009710.
Maier, U., and P. Grathwohl (2006), Numerical experiments and field results on the size of steady state plumes, *J. Contam. Hydrol.*, *85*(1–2), 33–52, doi:10.1016/j.jconhyd.2005.12.012.
Neuman, S. P., C. L. Winter, and C. M. Newman (1987), Stochastic theory of field-scale Fickian dispersion in anisotropic porous media, *Water Resour. Res.*, *23*(3), 453–466.
Pannone, M., and P. K. Kitanidis (1999), Large-time behavior of concentration variance and dilution in heterogeneous formations, *Water Resour. Res.*, *35*(9), 623–634.
Pollock, D. W. (1988), Semianalytical computation of path lines for finite-difference models, *Ground Water*, *26*(6), 743–750.
Prommer, H., B. Anneser, M. Rolle, F. Einsiedl, and C. Griebler (2009), Biogeochemical and isotopic gradients in a BTEX/PAH contaminant plume: Model-based interpretation of a high-resolution field data set, *Environ. Sci. Technol.*, *43*(21), 8206–8212, doi:10.1021/es901142a.

Rahman, M. A., S. C. Jose, W. Nowak, and O. A. Cirpka (2005), Experiments on vertical transverse mixing in a large-scale heterogeneous model aquifer, *J. Contam. Hydrol.*, *80*(3–4), 130–148.
Rajaram, H., and L. W. Gelhar (1995), Plume-scale dispersion in aquifers with a wide range of scales of heterogeneity, *Water Resour. Res.*, *31*(10), 2469–2482.
Ritzi, R., Z. Dai, D. Dominic, and Y. Rubin (2004), Spatial correlation of permeability in cross-stratified sediment with hierarchical architecture, *Water Resour. Res.*, *40*, W03513, doi:10.1029/2003WR002420.
Rolle, M., C. Eberhardt, G. Chiogna, O. A. Cirpka, and P. Grathwohl (2009), Enhancement of dilution and transverse reactive mixing in porous media: Experiments and model-based interpretation, *J. Contam. Hydrol.*, *110*(3–4), 130–142, doi:10.1016/j.jconhyd.2009.10.003.
Rolle, M., D. L. Hochstetler, G. Chiogna, P. K. Kitanidis, and P. Grathwohl (2012), Experimental investigation and pore-scale modeling interpretation of compound-specific transverse dispersion in porous media, *Transp. Porous Media*, *93*, 347–362.
Rolle, M., G. Chiogna, D. L. Hochstetler, and P. K. Kitanidis (2013), On the importance of diffusion and compound-specific mixing for groundwater transport: An investigation from pore to field scale, *J. Contam. Hydrol.*, *153*, 51–68, doi:10.1016/j.jconhyd.2013.07.006.
Rubin, Y. (1995), Flow and transport in bimodal heterogeneous formations, *Water Resour. Res.*, *31*(10), 2461–2468.
Rubin, Y. (2003), *Applied Stochastic Hydrogeology*, Oxford Univ. Press, Oxford, U. K.
Salandin, P., and V. Fiorotto (2000), Dispersion tensor evaluation in heterogeneous media for finite Peclet values, *Water Resour. Res.*, *36*(6), 1449–1455, doi:10.1029/2000WR900037.
Scheibe, T. D., and D. L. Freyberg (1995), The use of sedimentological information for geometric simulation of natural porous media structure, *Water Resour. Res.*, *31*(12), 3259–3270.
Scheidegger, A. E. (1961), General theory of dispersion in porous media, *J. Geophys. Res.*, *66*(10), 3273–3278.
Schwede, R. L., O. A. Cirpka, W. Nowak, and I. Neuweiler (2008), Impact of sampling volume on the probability density function of steady-state concentration, *Water Resour. Res.*, *44*, W12433, doi:10.1029/2007WR006668.
Srinivasan, V., T. P. Clement, and K. K. Lee (2007), Domenico solution—Is it valid?, *Ground Water*, *45*(2), 136–146, doi:10.1111/j.1745-6584.2006.00281.x.
Stauffer, F. (2007), Impact of highly permeable sediment units with inclined bedding on solute transport in aquifers, *Adv. Water Res.*, *30*(11), 2194–2201.
Stauffer, F., and M. Rauber (1998), Stochastic macrodispersion models for gravel aquifers, *J. Hydraul. Res.*, *36*(6), 885–896.
Thornton, S. F., S. Quigley, M. J. Spence, S. A. Banwart, S. Bottrell, and D. N. Lerner (2001), Processes controlling the distribution and natural attenuation of dissolved phenolic compounds in a deep sandstone aquifer, *J. Contam. Hydrol.*, *53*(3–4), 233–267, doi:10.1016/S0169-7722(01)00167-X.
Tonina, D., and A. Bellin (2008), Effects of pore-scale dispersion, degree of heterogeneity, sampling size, and source volume on the concentration moments of conservative solutes in heterogeneous formations, *Adv. Water Resour.*, *31*(2), 339–354, doi:10.1016/j.advwatres.2007.08.009.
Tukey, J. W. (1967), An introduction to the calculations of numerical spectrum analysis, in *Spectral Analysis of Time Series*, pp. 25–46, Wiley, N. Y.
Vanderborght, J. (2001), Concentration variance and spatial covariance in second-order stationary heterogeneous conductivity fields, *Water Resour. Res.*, *37*(7), 1893–1912.
Werth, C. J., O. A. Cirpka, and P. Grathwohl (2006), Enhanced mixing and reaction through flow focusing in heterogeneous porous media, *Water Resour. Res.*, *42*, W12414, doi:10.1029/2005WR004511.
Wexler, E. J. (1992), *Analytical Solutions for One-, Two-, and Three-Dimensional Solute Transport in Ground-Water Flow Systems with Uniform Flow, Applications of Hydraulics*, vol. 3, chap. B7, U.S. Geological Survey, Denver, Colo.
Willingham, T. H., C. J. Werth, and A. J. Valocchi (2008), Evaluation of the effects of porous media structure on mixing-controlled reactions using pore-scale modelling and micromodel experiments, *Environ. Sci. Technol.*, *42*(9), 3185–3193.
Zarlenga, A., and A. Fiori (2013), Steady plumes in heterogeneous porous formations: A stochastic Lagrangian approach, *Water Resour. Res.*, *49*, 864–873, doi:10.1002/wrcr.20106.
Zarlenga, A., I. Jankovic, and A. Fiori (2013), Advective transport in heterogeneous formations: The impact of spatial anisotropy in the breakthrough curve, *Transp. Porous Media*, *96*(2), 295–304.
Zhang, C., K. Dehoff, N. Hees, M. Ostrom, T. Wietsma, A. Valocchi, B. W. Fouke, and C. J. Werth (2010), Pore-scale study of transverse mixing induced $CaCO_3$ precipitation and permeability reduction in a model subsurface sedimentary system, *Environ. Sci. Technol.*, *44*, 7833–7838.